© 2014. Published by The Company of Biologists Ltd | Development (2014) 141, 1381-1391 doi:10.1242/dev.093435

RESEARCH ARTICLE

Wnt-regulated dynamics of positional information in zebrafish somitogenesis

Lola Bajard[1,*], Luis G. Morelli[1,2,‡,‡‡], Saúl Ares[2,§,‡‡], Jacques Pécréaux[1,¶], Frank Jülicher[2] and Andrew C. Oates[1,,§§]**

ABSTRACT

How signaling gradients supply positional information in a field of moving cells is an unsolved question in patterning and morphogenesis. Here, we ask how a Wnt signaling gradient regulates the dynamics of a wavefront of cellular change in a flow of cells during somitogenesis. Using time-controlled perturbations of Wnt signaling in the zebrafish embryo, we changed segment length without altering the rate of somite formation or embryonic elongation. This result implies specific Wnt regulation of the wavefront velocity. The observed Wnt signaling gradient dynamics and timing of downstream events support a model for wavefront regulation in which cell flow plays a dominant role in transporting positional information.

KEY WORDS: Fgf signaling, Wnt signaling, Embryonic elongation, Segmentation clock, Signal gradient, Time-lapse microscopy

INTRODUCTION

Segmentation of the anteroposterior axis is a widespread feature of animal body plans. Interpretation of positional information from signaling gradients (Aulehla and Pourquié, 2010; Chen et al., 2012; Porcher and Dostatni, 2010; Rogers and Schier, 2011) appears key in this process despite different modes of segmentation in different phyla. In the syncytial blastoderm of the fruit fly *Drosophila*, molecular signaling gradients supply positional information to initiate a hierarchical genetic cascade that simultaneously subdivides a body of fixed size into segments of similar length (Chen et al., 2012; Porcher and Dostatni, 2010). By contrast, vertebrate segmentation, known as somitogenesis, occurs sequentially and rhythmically at the posterior of a continually elongating body axis where multicellular blocks, known as somites, are periodically segregated from the anterior of the presomitic mesoderm (PSM) (Pourquié, 2011). Somitic precursor cells continuously join the posterior end of the PSM during elongation, creating an anteriorward cell flow through the PSM. Signaling gradients in the PSM are believed to supply positional information that regulates segment length (Aulehla and Pourquié, 2010), but how positional information is set in a continuous flow of cells remains unclear.

The rhythmicity of somitogenesis is governed by a segmentation clock consisting of cellular oscillators (Harima et al., 2013; Oates et al., 2012). Kinematic waves of oscillating gene expression sweep anteriorly across the PSM, arriving in the anterior as each new segment forms (Aulehla et al., 2008; Delaune et al., 2012; Masamizu et al., 2006; Palmeirim et al., 1997). These waves are believed to arise from the gradual slowing of oscillations in individual cells as they approach the anterior PSM (Morelli et al., 2009). This tissue-level pattern of oscillating gene expression is thought to repeat as each new somite forms, and the time interval of the repeat is termed the period of the segmentation clock.

The anteroposterior (A/P) length of a segment is proposed to be set when oscillating cells interact with a wavefront of cellular change that sweeps posteriorly down the axis (Cooke and Zeeman, 1976). In this scenario, which is termed the clock and wavefront mechanism, the wavefront converts the temporal information of the oscillating cells into a permanent segmental pattern (Oates et al., 2012). The clock and wavefront mechanism is a generic proposal about the dynamics of the system and, regardless of the molecular details, at steady state the segment length is fixed by the period of the segmentation clock and the wavefront velocity (Gomez et al., 2008; Morelli et al., 2009; Oates et al., 2012). Events associated with the wavefront include oscillation arrest and determination of segment boundary position; morphological somite formation is downstream of these rhythmic patterning events (Dahmann et al., 2011). It is therefore expected that segment length and the segmentation clock period are closely related to the morphologically observable somite length and somitogenesis period, respectively.

The currently favored hypothesis for how wavefront velocity is regulated involves gradients of Wnt, fibroblast growth factor (Fgf) and retinoic acid (RA) spanning the PSM (reviewed by Aulehla and Pourquié, 2010). Wnt and Fgf ligands are transcribed in the regressing tailbud and are thought to build gradients by gradual decay of ligand mRNA and/or protein in the cell flow across the PSM (Aulehla et al., 2003; Dubrulle and Pourquié, 2004). The contribution of potential ligand diffusion (Yu et al., 2009) to the shape of the gradients, or to the downstream gradients of signal reception, has not been examined. It remains difficult to interpret the effects of perturbations to these signaling gradients in regulating wavefront velocity because Wnt, Fgf and RA also play important roles in embryonic elongation and posterior body development (Wilson et al., 2009). Experimental uncoupling of gradient dynamics from posterior development and elongation of the embryo would simplify interpretation. Furthermore, to interpret changes in segment length resulting from signaling gradient perturbation, wavefront

[1]Max Planck Institute of Molecular Cell Biology and Genetics, Pfotenhauerstrasse 108, D-01307 Dresden, Germany. [2]Max Planck Institute for the Physics of Complex Systems, Nöthnitzer Strasse 38, D-01187 Dresden, Germany. *Present address: CEITEC-Central European Institute of Technology, Masaryk University, Kamenice 735/5, 62500 Brno, Czech Republic. ‡Present address: Departamento de Física, FCEyN Universidad de Buenos Aires, and IFIBA, CONICET, Pabellón 1, Ciudad Universitaria, 1428 Buenos Aires, Argentina. §Present address: Logic of Genomic Systems Laboratory, Spanish National Centre for Biotechnology CNB-CSIC, E-28049 Madrid, Spain. ¶Present address: Institute of Genetics and Developmental Biology of Rennes, CNRS UMR 6290, University Rennes 1, 2 Avenue du Prof. L. Bernard, 35043 Rennes, France. **Present address: MRC-National Institute for Medical Research, The Ridgeway, Mill Hill, London NW7 1AA, UK. ‡‡These authors contributed equally to this work

§§Author for correspondence (aoates@nimr.mrc.ac.uk)

Received 19 December 2012; Accepted 21 January 2014

Development (2014) doi:10.1242/dev.093435

velocity and clock period must be simultaneously assessed. To date, these criteria have not been met in any system and the specific roles of Wnt, Fgf or RA in supplying positional information in somitogenesis remain unclear (Oates et al., 2012). Although the wavefront may be influenced by each of these signals, here we focus on the role of Wnt signaling in regulating wavefront velocity.

Current understanding of the role of Wnt in regulating the wavefront comes from experiments in mouse and chick embryos. A qualitative gradient of Wnt signaling activity has been reported across the mouse PSM, with highest levels in the posterior (Aulehla et al., 2008). Ubiquitously active Wnt signaling in the mouse PSM dramatically changes the position of oscillator arrest, creating a longer PSM (Aulehla et al., 2008; Dunty et al., 2008). Furthermore, implantation of Wnt3-overexpressing cell clusters in chick PSM shifts the locally forming somite boundary anteriorly (Aulehla et al., 2003). Consistent with these observations, it was proposed that posterior PSM cells are maintained in an undetermined and oscillating state by high levels of Wnt signaling, and that the wavefront is triggered directly in anterior PSM below a concentration threshold in a Wnt activity gradient spanning the PSM (Aulehla and Herrmann, 2004; Aulehla et al., 2003). However, in the absence of quantitative analysis of the signaling gradient and the timing of its downstream targets during segmentation, it is still an open question as to when and where Wnt signaling supplies positional information to the flow of cells in the PSM.

Here, using time-controlled manipulation of Wnt signaling and time-lapse imaging of live zebrafish embryos, we define conditions under which wavefront velocity can be tuned without perturbing embryonic elongation or somitogenesis period, resulting in segments of abnormal length. Measurements of the distribution and dynamics of the Wnt signaling gradient, as well as the timing of downstream events, reveal that the wavefront is not triggered directly in the anterior PSM by a Wnt activity threshold. Instead, our results support a model in which Wnt-regulated positional information in the posterior PSM is relayed and refined by downstream targets and is transported by cell flow to the anterior PSM.

RESULTS

Time-controlled Wnt modulations affect somite length

A role for Wnt signaling in zebrafish segmentation is not yet established, partly owing to evolutionarily conserved early roles in A/P axis specification (Shimizu et al., 2005; Thorpe et al., 2005) and later axial elongation (Martin and Kimelman, 2009; Martin and Kimelman, 2012). To avoid these roles of Wnt, we explored time-controlled inhibition or activation of the Wnt pathway during somitogenesis. We used heat shock-inducible transgenes expressing either Axin1, an intracellular inhibitor of the pathway (Kagermeier-Schenk et al., 2011); Dkk1, an extracellular inhibitor (Stoick-Cooper et al., 2007); or Wnt8, a ligand (Weidinger et al., 2005). Transgenic embryos and their wild-type (WT) siblings were briefly heat shocked during trunk somitogenesis (1- to 9-somite stage), then elongation and somite length were measured from brightfield time-lapse movies of multiple embryos developing simultaneously. We measured the elongation velocity e relative to a reference point in the already formed somites, along the line of the axis (Fig. 1A,B, white line).

Inhibition of Wnt signaling by *axin1* overexpression dramatically slowed embryonic elongation, thus preventing specific analysis of segmentation (supplementary material Fig. S1A-C′, Movie 1). Consistent with previous work, overexpressing Dkk1 at the 1-somite stage also led to posterior truncation (Martin and Kimelman, 2012); however, elongation was not slowed until the twelfth to thirteenth somite post-heat shock (phs) (Fig. 1A-C′; supplementary material Table S1, six out of seven experiments), leaving the interval up to 13 somites phs open for segmentation analysis. Wnt8 induction did not affect elongation.

We observed significant changes in somite length following overexpression of Dkk1 or Wnt8 (Fig. 1A′,B′,D; supplementary material Fig. S1D-G, Movies 2, 3) compared with WT siblings, starting ~8 somites phs (Fig. 1D; supplementary material Fig. S1F,G). Inhibition of Wnt signaling by Dkk1 overexpression led to the systematic formation of up to six longer somites starting eight somites phs [Fig. 1D; 21±7% longer (mean ± s.d.), seven independent experiments, n=50]. These effects were consistent for heat shocks delivered at 1- to 9-somite stages. Activation of Wnt signaling by Wnt8 overexpression had the opposite effect: formation of up to three smaller somites (supplementary material Fig. S1F,G; ninth somite 14±6% smaller, four independent experiments, n=29). Although the eighth and ninth somites phs were smaller in all experiments, this effect was not fully penetrant.

In all transgenic and WT embryos, the sixth somite formed phs was significantly shorter and sometimes followed by a longer somite (Fig. 1D; supplementary material Fig. S1F). This effect was due only to the heat shock, and proved a useful temporal mark to compare experiments. As a long-term effect, shorter somites formed after Dkk1 overexpression starting at ~17 somites phs (Fig. 1D), possibly as a consequence of the system's recovery. However, because of associated effects on tail outgrowth at these later stages interpretation is complicated. We conclude that time-controlled modulation of the canonical Wnt pathway by Dkk1 or Wnt8 induction during somitogenesis modifies somite length, starting eight somites phs, without affecting embryonic elongation.

To test whether this effect on somite length results from an earlier defect in segmental patterning, we measured the distance between *mespb* gene expression stripes in the anterior PSM. *mespb* is a marker and determinant of the rostral compartment of the presumptive somites of zebrafish (Sawada et al., 2000) and other vertebrate species (Buchberger et al., 2000; Saga et al., 1997). In zebrafish, the distance between the posterior two stripes is one of the earliest markers of segment length [presumptive somite –I, where somite I is the most recently formed somite (Pourquié and Tam, 2001)] (Fig. 1E,F; supplementary material Fig. S1H,I). At 3.5 hours (~7 somite cycles) phs, the length of the *mespb* interstripe was 32±24% larger after Wnt inhibition and 14±9% smaller after Wnt activation (Fig. 1E-G; supplementary material Fig. S1H-J). These values are qualitatively consistent with the effects on somite length and show that segment length in the anterior PSM had already been altered ~6 somites after heat shock modulation of Wnt signaling (Fig. 1G; supplementary material Fig. S1J). In conclusion, these results are the first evidence that Wnt regulates segmentation in zebrafish.

Wnt inhibition does not alter somitogenesis period but increases the rate of PSM shortening

The change in segment length that we observed could have resulted from a modification in the clock period T and/or the wavefront velocity v. From time-lapse movies, we measured the period of somitogenesis T_s by calculating the slope of the linear increase in somite number versus time (Fig. 2A,A′) (Schröter et al., 2008). We use this period as a proxy for segmentation clock period. Because effects on somite length using Wnt8 overexpression were not fully penetrant and generally restricted to two somites, we only analyzed Dkk1 overexpression. We delivered heat shocks in separate experiments between the 1- and 9-somite stages and measured T_s during the formation of the longer somites, which always occurred

Development (2014) doi:10.1242/dev.093435

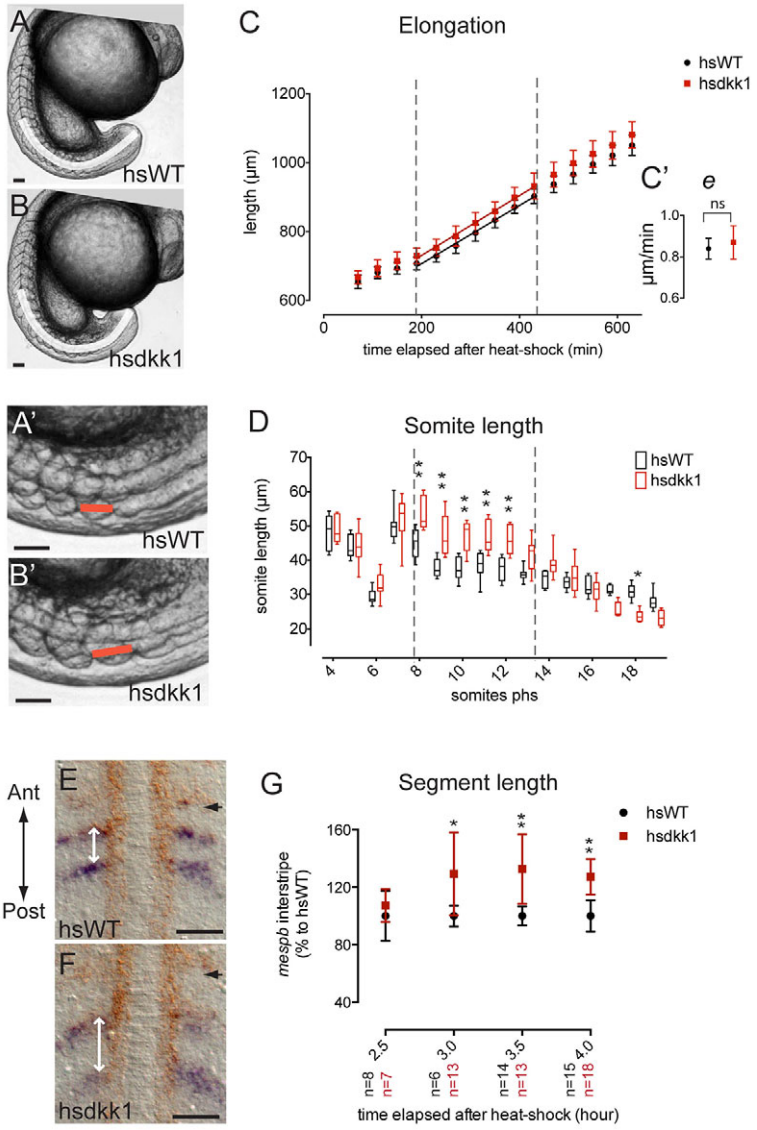

Fig. 1. Reduction of Wnt signaling during trunk somitigenesis using *hsdkk1* transgene preserves elongation and increases somite length. *hsdkk1::GFP* heterozygote outcross. (A-D) Posterior elongation and instantaneous somite length over time, showing a representative experiment with heat shock at ~9 somites; *n*=8 per condition. Lateral view of representative heat shocked (hs) wild-type (WT) control (A) or transgenic (B) embryo, with magnification of the last three somites formed (A′,B′) when the tenth somite post-heat shock (phs) forms. (C) Plot of distance between fixed position in somites and posterior tip (white line in A,B) over time. (C′) Elongation rate, 190-430 minutes phs. (D) Box plot of instantaneous somite length (distance between consecutive notches, orange line in A′,B′). (E,F) Dorsal view of flat-mounted anterior PSM of control or transgenic embryo double-stained for *mespb* (blue) and *myoD* (red), fixed 4 hours phs. Black arrow indicates the last-formed somite. (G) Segment length (distance between two *mespb* stripes, white arrow in E,F) in embryos fixed every 30 minutes after heat shock, starting 2.5 hours phs. Mean ± s.d. **P*<0.01, ***P*<0.001; ns, not significant. Scale bars: 50 µm. See also supplementary material Fig. S1, Table S1, Movies 1-3.

8-13 somites phs (Fig. 2A, dashed lines). We observed no significant increase in somitogenesis period (six out of seven experiments; Fig. 2A′; supplementary material Table S1). This suggests that the increase in somite length is not a consequence of an altered clock period.

We next investigated wavefront velocity as the other potential cause of change in segment length. Because the molecular events associated with the underlying wavefront are not visible in brightfield images, we first measured the progress of a morphological wavefront of somite boundary formation. The morphological wavefront velocity v_m (which anteriorly reduces PSM length) and the elongation velocity e (which posteriorly increases PSM length) combine to set PSM length L (Fig. 2B). If both velocities are equal, PSM length stays constant. However, this is not the case over longer developmental times, when PSM length changes in mouse, chick, snake and fish embryos (Gomez et al., 2008; Schroter and Oates, 2010).

The change in PSM length dL/dt measured from time-lapse movies was significantly increased after Wnt inhibition in six out of seven experiments (Fig. 2C,C′; supplementary material Table S1). To estimate the morphological wavefront velocity v_m, we subtracted dL/dt from the values of elongation measured above. This showed that v_m was increased by 17±10% (Fig. 2D; seven independent experiments, n=50; supplementary material Table S2). The increase in v_m was greater for early- to mid-trunk somitogenesis (30±13%) than for late trunk somitogenesis (14±9%). We then used our measurements of somite length S and somitogenesis period T_s for an independent estimate of v_m using $v_m=S/T_s$ (supplementary material Table S2). With this method, we found a consistent increase of 21±14% after Wnt inhibition. Combined, these results reveal for the first time a specific alteration to morphological wavefront velocity in response to an alteration in Wnt signaling.

Determination front and oscillation arrest shift position after Wnt inhibition

If our measurements at the morphological level reflect a change in the underlying wavefront velocity, we would expect to see a corresponding positional change in segment determination and oscillator arrest in the anterior PSM. We therefore examined segment polarity and oscillating gene expression by *in situ* hybridization in embryos fixed during specification of the larger segments.

We used the position of the posteriormost *mespb* stripe in the PSM as a marker of the determination front, as previously (Herrgen

Development (2014) doi:10.1242/dev.093435

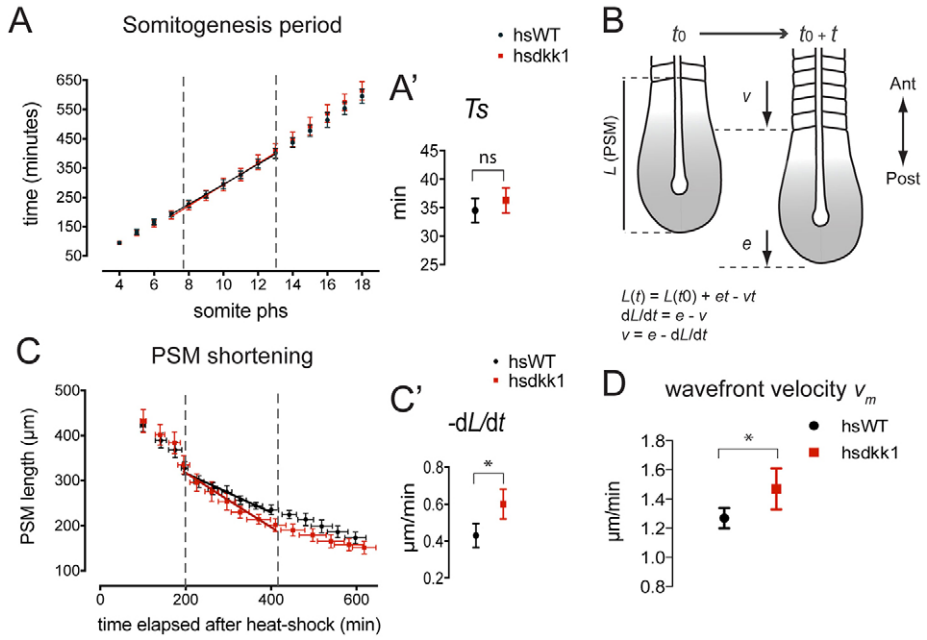

Fig. 2. Wnt inhibition increases the velocity of morphological wavefront regression without affecting somitogenesis period. (A) Timing of somite boundary formation from fourth somite after heat shock. (A′) Somitogenesis period T_s from the seventh to the thirteenth somite phs. (B) PSM length *L* is increased by posterior elongation *e* and decreased by morphological wavefront regression during time interval *t*. Underlying wavefront velocity *v* is inferred from elongation minus the rate of change in PSM length. (C) Distance between the posterior boundary of last formed somite and posterior tail tip measured each time a new somite forms. (C′) Rate of change of PSM length *dL/dt* between formation of seventh and thirteenth somites (~200-400 minutes) phs. (D) Morphological wavefront velocity v_m=*e* –*dL/dt*. Mean ± s.d.; *n*=8 for hsWT, *n*=8 for hsdkk1. **P*<0.01. See supplementary material Tables S1, S2.

et al., 2010; Schroter and Oates, 2010). At 3.5 hours (~7 somites) phs, the distance between the *mespb* stripe and the posterior end of the notochord was shorter in *hsdkk1* transgenics than in WT littermates (91±9%, *n*=18; Fig. 3A-E). Time series analysis revealed that the effect started at 3 hours (~6 somites) phs (Fig. 3E). This suggests that the position of the determination front is shifted posteriorly in the PSM by a reduction in Wnt signaling.

We next asked whether the position of oscillation arrest is also shifted posteriorly in response to Dkk1 induction. We examined expression of the cyclic genes *her1*, *her7* and *dlc*. All are still expressed 3.5 hours (~7 somites) after heat shock induction of Dkk1 (Fig. 3F-I; supplementary material Fig. S2A-D; data not shown). We observed different phase patterns among Dkk1-expressing embryos within the same clutch, indicating that cyclic genes were oscillating. We estimated the length of the oscillating domain using the distance from the posterior end of the notochord to the anterior margin of the anteriormost cyclic expression stripe of *her7*. The position of cyclic gene expression stripes in the PSM is thought to change continuously through the segmentation clock cycle. To accurately estimate changes, it is important to compare gene expression stripes in different embryos at similar cycle phases. We subdivided the embryos into two phase-matched groups: those with three stripes (Fig. 3F,H) and those with two stripes (Fig. 3G,I). The distance to the anteriormost stripe was shorter after heat shock in *hsdkk1* embryos than in WT littermates for both the two- and three-stripe categories (supplementary material Fig. S2E), indicating that the length of the oscillating domain is reduced. Indeed, this effect was strong enough to be observed when embryos were pooled regardless of phase. A decrease in oscillating domain length was also systematically observed in several experiments using *dlc* and *her1* (supplementary material Fig. S2F; data not shown). A time series from pooled embryos with two or three stripes showed that the arrest front begins to shift ~3 hours (~6 somites) phs (Fig. 3J). Thus, although the exact location of oscillator arrest relative to the anteriormost *her7* stripe is not known, this result suggests that the position of oscillator arrest in the PSM shifts posteriorly after Wnt inhibition.

Together, these results demonstrate that Dkk1 overexpression controls the position of molecular markers of the wavefront in the

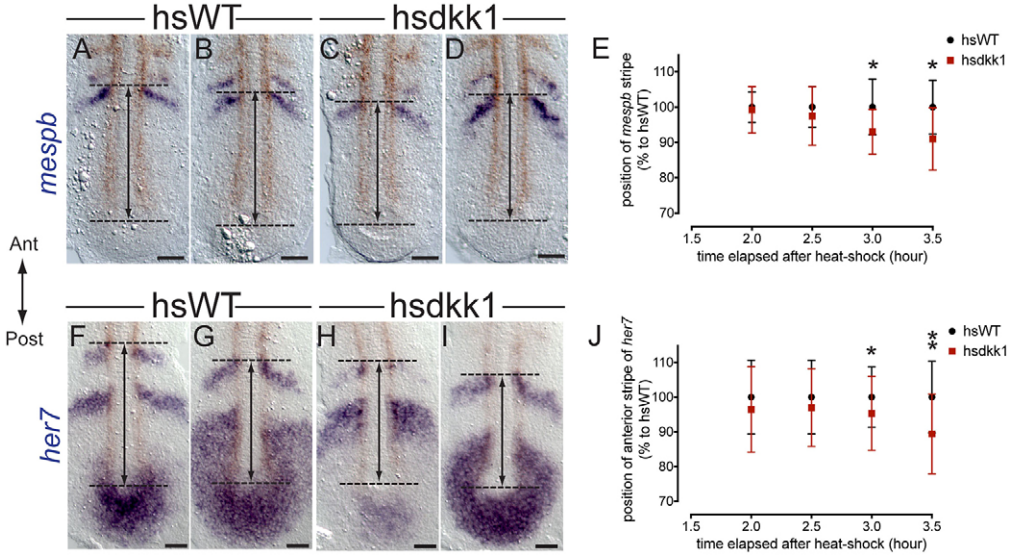

Fig. 3. Wnt inhibition shifts the position of molecular markers of the wavefront posteriorly ~6 somites after heat shock. (A-D,F-I) Dorsal view of flat-mounted hsWT (A,B,F,G) or hsdkk1 (C,D,H,I) PSM heat shocked at six somites (A-D) or one somite (F-I), fixed 3.5 hours phs and hybridized with *mespb* (A-D) or *her7* (F-I) probes. (E,J) Normalized distance between posterior *mespb* stripe (E) or anteriormost *her7* stripe (J) and the posterior end of the notochord (black arrows in A-D,F-I) at successive time points. Mean ± s.d. **P*<0.01, ***P*<0.001. Scale bars: 50 µm. See supplementary material Fig. S2.

Development (2014) doi:10.1242/dev.093435

PSM. From the consistent morphological and molecular changes observed in our assay, we infer that Wnt signaling has a specific role in regulating wavefront velocity in zebrafish.

The Wnt activity gradient is restricted to posterior PSM and is reduced hours before wavefront markers are shifted

How does Wnt activity instruct the position of the wavefront within the PSM? Previous studies have suggested that the levels of Wnt ligand or downstream effects are graded in mouse and zebrafish (Aulehla and Pourquié, 2010; Aulehla et al., 2003; Aulehla et al., 2008; Row and Kimelman, 2009; Thorpe et al., 2005), but quantitative analysis of the distribution and timing of Wnt activity is still lacking. The intracellular response to canonical Wnt binding its receptor includes translocation of β-catenin to the nucleus (Chien et al., 2009), and thus β-catenin concentration in the nucleus indicates canonical Wnt signaling activity. We examined the spatial distribution of Wnt signaling activity in the PSM using fluorescence immunohistochemistry against β-catenin. As a constituent of the cytoskeleton, β-catenin also gives a cortical signal in all embryonic cells (supplementary material Fig. S3B). We therefore developed an image processing procedure to estimate nuclear β-catenin concentration along the A/P axis (supplementary material Fig. S3).

We examined normally developing embryos during mid-trunk somitogenesis and observed a gradient of nuclear β-catenin fluorescence intensity, with highest levels in the tailbud and posterior PSM and lower levels more anteriorly (Fig. 4A,C,D). Importantly, a basal level was reached at ~50% of PSM length as measured from the tail tip, and the intensity profile was flat in the anterior half of the PSM (Fig. 4D). This distribution of nuclear β-catenin is consistent with the posteriorly restricted expression of both *wnt3a* and *wnt8* genes and known Wnt target genes in the zebrafish tailbud, such as *ntl* or *axin2* (supplementary material Fig. S4) (Jho et al., 2002; Kelly et al., 1995; Lekven et al., 2001; Martin and Kimelman, 2012; Shimizu et al., 2005; Stulberg et al., 2012). By contrast, the nuclear β-catenin fluorescence intensity is not graded in the anterior PSM, where oscillators arrest and markers of segmental determination such as *mespb* are expressed (Fig. 4B,D).

We next measured the response of the nuclear β-catenin gradient to time-controlled perturbation of Wnt signaling in our assay. The maximum levels of nuclear β-catenin in the tailbud were reduced to ~60% between 30 minutes and 1 hour after the *dkk1GFP* heat shock when compared with control embryos, and the position where signaling activity reached basal levels was shifted posteriorly (Fig. 4E-K). Thus, inhibition of Wnt in our assay was already effective 1 hour (~2 somites) phs. This corresponds to a four to five somite delay between when Wnt signaling is reduced in the posterior and when wavefront markers are affected in the anterior PSM.

We conclude that the observed posterior distribution of the nuclear β-catenin gradient in the WT zebrafish embryo and the timing of its response to perturbations in Wnt signaling during somitogenesis are inconsistent with the regulation of the wavefront by Wnt signaling occurring in the anterior PSM.

Fgf signaling is weakly affected downstream of time-controlled Wnt inhibition

Our results suggest that the Wnt signaling gradient might be instructing a cellular decision in posterior PSM that is relayed or transported by intermediate players into anterior PSM. The expression or activity of such candidates should be affected after Wnt perturbation, but before observed changes to the anterior wavefront markers, and have a connection to wavefront activity.

The Fgf pathway is proposed to be a regulator of the wavefront in mouse, chick and zebrafish, and in mouse was reported to be

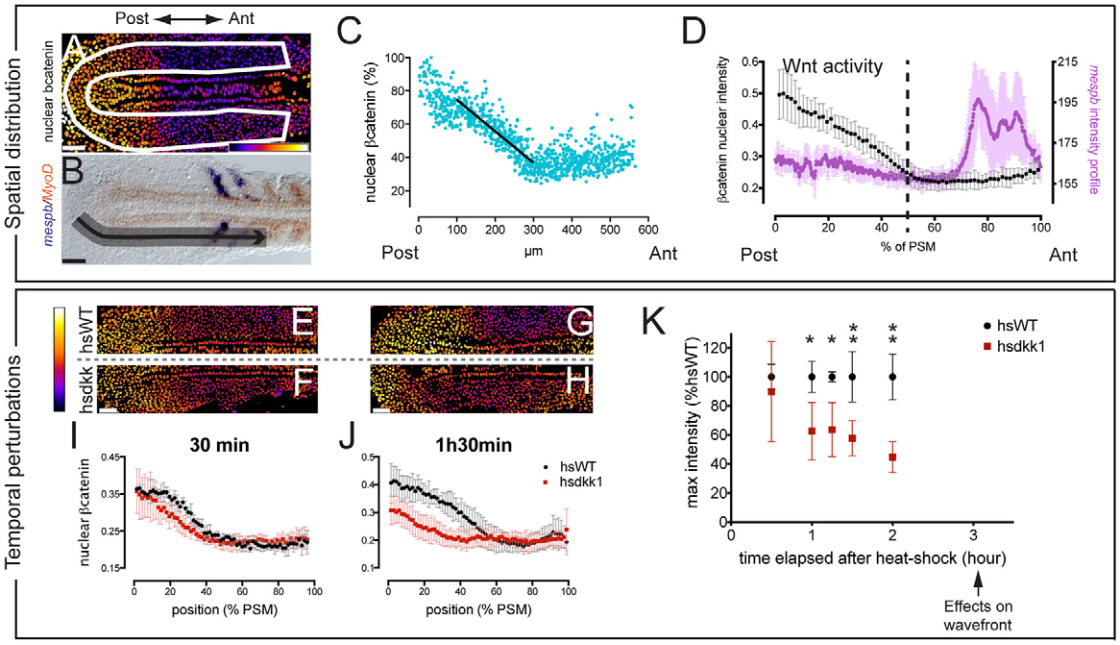

Fig. 4. A posterior gradient of Wnt activity is reduced ~2 somites after heat shock. (A,B,E-H) Dorsal view of flat-mounted non-heat shocked (A,B), hsWT (E,G) or hsdkk1 (F,H) PSM at nine (G,H), ten (A,E,F) or 12 (B) somites. Embryos were fixed 30 minutes (E,F) or 1.5 hours (G,H) phs. (A) Fluorescence intensity of β-catenin staining after applying a nuclear mask, displayed using false color. (B) Whole-mount *in situ* hybridization with *mespb* (blue) and *myoD* (red) probes. (C,D,I,J) Nuclear intensity of β-catenin staining (C, percentage of maximum; D,I,J, grayscale values) along the PSM length for individual cells, for one embryo (C) or averaged within 1.5% bins for several embryos (D,I,J). Error bars reflect variation between embryos. The average *mespb* intensity profile is in purple in D. (K) Maximum intensity nuclear β-catenin normalized to hsWT dynamic range, with embryos fixed at successive time points. Mean ± s.d. **P*<0.01, ***P*<0.001. Scale bars: 50 μm. See also supplementary material Figs S3, S4.

Development (2014) doi:10.1242/dev.093435

regulated by Wnt signaling (Aulehla et al., 2003; Aulehla et al., 2008; Dubrulle et al., 2001; Dunty et al., 2008; Naiche et al., 2011; Sawada et al., 2001; Wahl et al., 2007). To investigate whether Wnt inhibition affects the wavefront by reducing Fgf signaling in our assay in zebrafish, we first asked whether Dkk1 overexpression alters mRNA expression of Fgf pathway members. *In situ* hybridization with NBT/BCIP color development is not quantitative for mRNA level, but short color development times can be used to detect relative changes and spatial gradients (Dubrulle et al., 2001; Dubrulle and Pourquié, 2004; Picker et al., 2009). We did not observe a reduction in staining intensity of *fgf3*, *fgf8* or *fgf receptor 1* (*fgfr1*) riboprobes in the PSM by *in situ* hybridization during the timecourse of our assay (Fig. 5A-D; supplementary material Fig. S5A-F). Nor did we find reduced expression levels in the PSM of two Fgf target genes: *pea3* and *erm* (also known as *etv4* and *etv5b*) (Fig. 5E-H; supplementary material Fig. S5G-J). We did, however, observe an increase in *erm* riboprobe staining intensity in the posterior tailbud (Fig. 5G,H; supplementary material Fig. S5I,J) and a decrease in *fgf8* riboprobe staining intensity in the mid-hindbrain boundary (supplementary material Fig. S5E,F), implying that color development had a suitable dynamic range in these experiments. Although small changes in mRNA levels in the PSM cannot be ruled out, these data suggest that reduction of Wnt signaling in this assay does not cause major alterations in the gene expression of Fgf pathway components.

To directly and quantitatively examine the timecourse of Fgf intracellular signaling activity in our assay, we visualized doubly phosphorylated Erk (dpErk) by fluorescence immunohistochemistry. Downstream of Fgf receptor activation, Erk kinase becomes rapidly phosphorylated, and dpErk levels have been used to monitor Fgf signaling in zebrafish (Sawada et al., 2001; Stulberg et al., 2012). In WT embryos at ten somites, the dpErk signal was distributed in a striking bi-modal profile (Fig. 5I,J). Highest levels were observed at ~25% of PSM length, corresponding to the posterior end of the notochord; posteriorly, a graded signal decreased to about half-maximum at the tip of the tailbud, and anteriorly the signal was at background levels at ~60% of PSM length. More anteriorly, an increase in dpErk signal was seen; this is associated with myogenesis in the forming somites (Groves et al., 2005).

We assessed the effect of Dkk1 overexpression on dpErk levels by comparing both the maximum intensity of the dpErk signal and the PSM location at which the anterior dpErk gradient dropped to

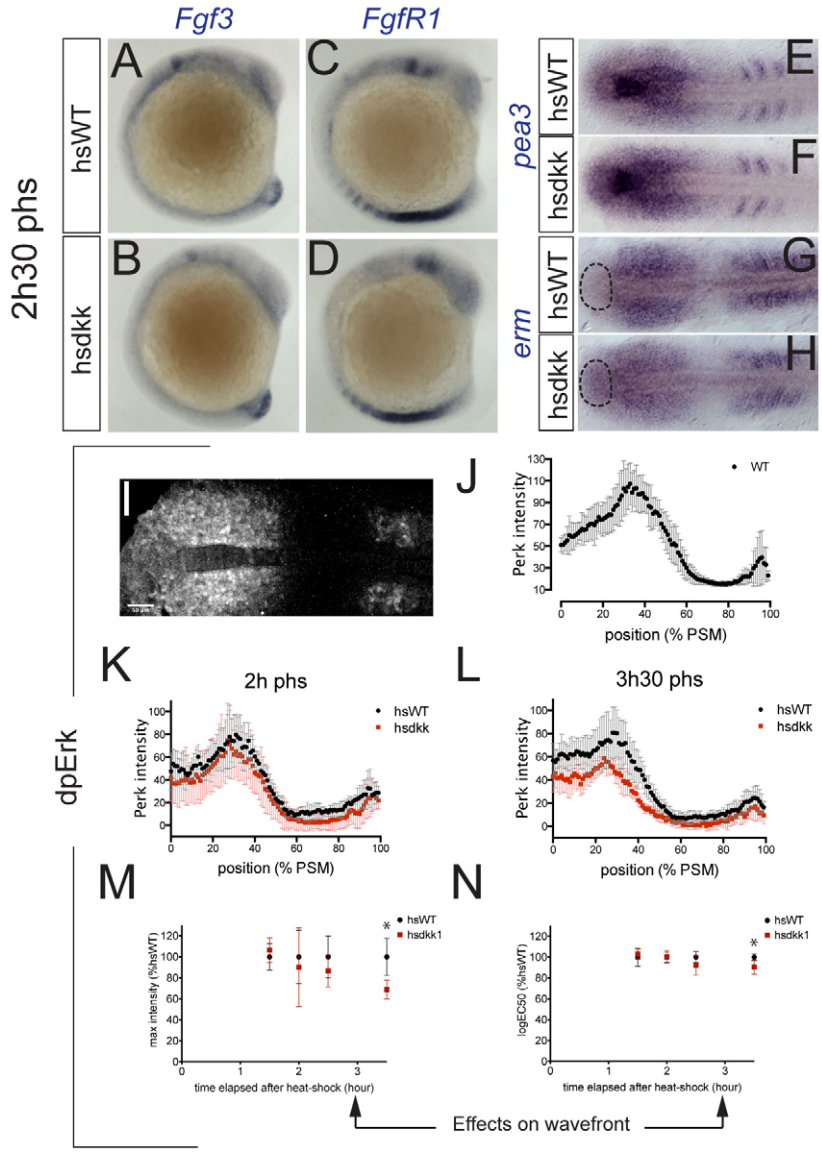

Fig. 5. Fgf activity is weakly reduced ~7 somites after heat shock. (A-D) Lateral view of *hsdkk1::*GFP (B,D) or WT siblings (A,C) heat shocked at eight somites, fixed 2.5 hours phs and hybridized with *fgf3* (A,B) or *fgfr1* (C,D) riboprobes. (E-H) Dorsal view of flat-mounted PSM from *hsdkk1::*GFP (F,H) or WT siblings (E,G) heat shocked at eight somites, fixed 2.5 hours phs and hybridized with *pea3* (E,F) or *erm* (G,H) riboprobes. Dashed outline indicates domain of expression elevated in *hsdkk1* embryos. (I) Confocal section of flat-mounted PSM of 10-somite stage WT immunostained with dpErk antibody. (J) Average gray value intensity profile of dpErk signal in 10-somite stage WT embryos. (K,L) *hsdkk1::*GFP or WT siblings, heat shocked at six somites and fixed 2 (K) or 3.5 (L) hours phs, showing percentage of dpErk signal relative to hsWT dynamic range. (M,N) Time series after heat shock of maximum intensity (M) or logEC50 (N) from plots of dpErk signal normalized to hsWT. Mean ± s.d. *P<0.01.

Development (2014) doi:10.1242/dev.093435

50% relative intensity (logEC50) at intervals phs. We observed no difference in either measure before 3.5 hours phs (Fig. 5K,M,N), by which time changes to segment determination and cyclic gene expression had already occurred in the anterior PSM (Fig. 3). At 3.5 hours phs, we detected a significant decrease in the maximum intensity of dpErk signal and logEC50 of the gradient (Fig. 5L-N). Although these data do not exclude some contribution, together they argue against a major role of Fgf signaling in mediating the effects of canonical Wnt signaling on the wavefront in our assay.

Reduction in *spadetail* and *mesogenin 1* expression after Wnt inhibition precedes the shift in wavefront markers

We next examined the expression timecourse of the transcription factor genes *spadetail* (*spt*; also known as *tbx16*) and *mesogenin 1* (*msgn1*) in the PSM following Dkk1 overexpression. *Msgn1* is a Wnt target gene in mouse (Wittler et al., 2007) and *spt* is downstream of Wnt signaling in zebrafish (Szeto and Kimelman, 2004; Thorpe et al., 2005). Msgn1, together with Spt, induces *tbx6* (also known as *fused somites* or *tbx24*) expression (Fior et al., 2012; Yabe and Takada, 2012), which is a well-established regulator of segmental determination (Holley et al., 2000; Nikaido et al., 2002; Oates et al., 2005; van Eeden et al., 1996).

Whole-mount *in situ* hybridization revealed that the *spt* expression domain decreases after Dkk1 overexpression (Fig. 6A-D). To determine the timing of this change, we plotted the intensity profiles for several embryos and measured the length of the expression domain (Fig. 6E-G). This revealed a posterior shift in *spt* expression starting between 2 and 2.5 hours (four to five somites) phs, ~1.5 hours after the effect on nuclear β-catenin and 1 hour before the effect on the wavefront (Fig. 6A-G). Similarly, inhibition of Wnt signaling led to downregulation of *msgn1* expression (Fig. 6H-M) between 2 and 2.5 hours (four to five somites) phs (Fig. 6N). Thus, *msgn1* expression is also downstream of changes to the Wnt activity gradient and upstream of changes to the wavefront during segmentation. We conclude that the Msgn1 and Spt transcription factors are plausible candidates to relay posterior Wnt-mediated positional information to the anterior PSM.

Transport of Wnt-mediated positional information from posterior to anterior by cell flow

Finally, we asked whether cell flow in the PSM could contribute to the spatiotemporal changes following heat shock (Fig. 7). The timecourse of changes we have observed after Wnt perturbation delineates a successive chain of events across the PSM with a total duration of ~4 hours (~8 somites). From the timing (4 hours) and the distance from the start of a linear Wnt activity gradient to the anterior end of the PSM at ~14 somites (~300 µm), we estimate the velocity with which the changes propagate across the PSM following a reduction in Wnt signaling activity as ~1.25 µm/minute. Assuming a constant and linear cell flow in the region of interest (Morelli et al., 2009), we approximated the magnitude of cell flow velocity in the PSM using the elongation velocity measured from time-lapse microscopy (supplementary material Table S1); this value is ~1.0 µm/minute, in good agreement with the velocity of information propagation. Thus, a simple transport process of cell flow in the PSM could account for the observed velocity of information propagation. Additional, faster processes, such as signaling relays or diffusion, need not be considered. In other words,

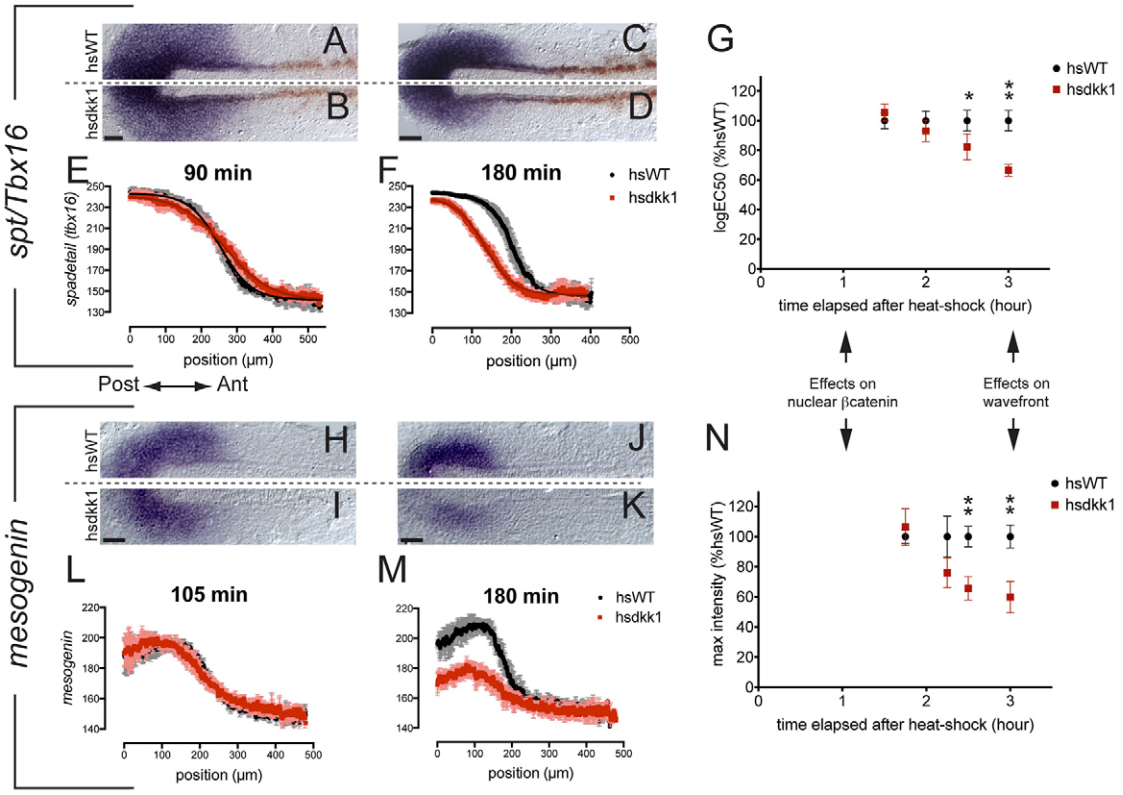

Fig. 6. Wnt target gene expression is reduced four to five somites after heat shock. (A-D,H-K) Dorsal view of flat-mounted PSM from *hsdkk1:*::GFP (B,D,I,K) or WT siblings (A,C,H,J) heat shocked at five (A-D) or six (H-K) somites, fixed 1.5 (A,B), 1.75 (H,I) or 3 (C,D,J,K) hours phs and hybridized with *spt* (A-D) or *msgn1* (H-K) riboprobes. (E,F,L,M) Average intensity profile for *spt* (E,F) and *msgn1* (L,M) along the A/P axis. (G) Normalized logEC50 calculated from fitting plots of *spt* intensity profile at successive time points. (N) Maximum intensity of *msgn1* normalized to hsWT dynamic range at successive time points. Mean ± s.d. **P*<0.01, ***P*<0.001. Scale bars: 50 µm.

Development (2014) doi:10.1242/dev.093435

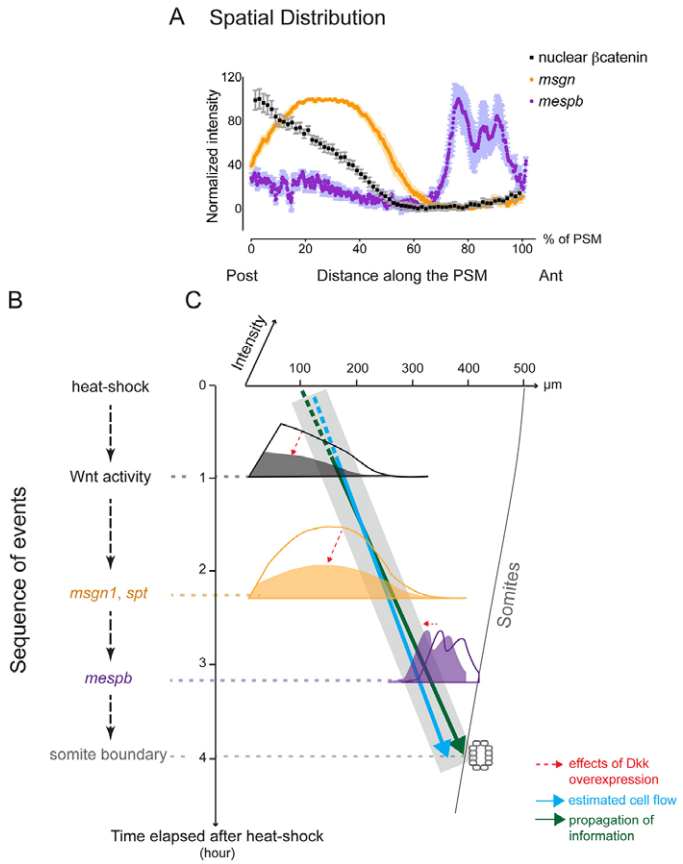

Fig. 7. Model for Wnt regulation of positional information in the PSM. (A) Spatial distribution of the Wnt signaling cascade. Illustration of nuclear β-catenin, *msgn1* and *mespb* profiles along the PSM. (B) Sequence of events down the Wnt signaling cascade following heat shock. (C) Information propagation across the PSM. The thin black line (right) illustrates the reduction in PSM length. Distributions of Wnt activity (black), downstream target *msgn1* (orange), wavefront markers *mespb* (purple) and formed somites are indicated at the time when the effects are first observed following heat shock. The red dashed arrow illustrates the effect of Dkk1 overexpression. Gray shading highlights the correspondence between cell flow (blue arrow) and information propagation (green arrow) velocity.

a cell located in the Wnt activity gradient in the posterior PSM at the time of heat shock would be swept with the cell flow into the anterior PSM with the correct timing to participate directly in the observed alterations to segment length.

DISCUSSION

Tuning wavefront velocity independently of clock period and elongation

Canonical Wnt signaling is well known for its role in the formation and later development and elongation of the posterior body structures, including the PSM (Greco et al., 1996; Martin and Kimelman, 2009; Martin and Kimelman, 2012). The difficulty in dissociating these Wnt functions from those in PSM patterning has blocked specific analysis of Wnt in segmentation in zebrafish. In mouse, evidence for a specific role first came from a *Wnt3a* hypomorph in which defects in posterior development appeared after segmentation had already started, leaving a time window for analysis (Aulehla et al., 2003). Here we temporally dissociate effects on segmentation from effects on posterior development and elongation using a time-controlled mild perturbation of the Wnt pathway. This perturbation is a distinctive test of the clock and wavefront mechanism (Cooke and Zeeman, 1976). Previous work indicated that segment length can be altered by changing the clock period while leaving wavefront velocity unchanged (Harima et al., 2013; Herrgen et al., 2010; Schroter and Oates, 2010). Here, we achieve the same outcome by altering wavefront velocity while leaving clock period unchanged. This apparent independence of clock period and wavefront velocity is difficult to reconcile with any model of somitogenesis in which the wavefront arises from coupling between oscillators and in which the period is strictly dependent on the wavefront velocity (Murray et al., 2011).

In chick and mouse there is some evidence for Wnt regulation of the segmentation clock period (Gibb et al., 2009). Although our results do not rule out a function of Wnt signaling in regulating the segmentation clock period in zebrafish, they are consistent with a conserved role for Wnt in regulating wavefront velocity throughout vertebrates.

A posterior Wnt signaling gradient imparts positional information

How does the Wnt signaling gradient regulate the dynamics of wavefront position? The simplest model proposed that local levels of Wnt activity in the anterior PSM directly define the wavefront position: PSM cells arrest oscillations and define their position in the future somite once they reach a given threshold in the anterior PSM in a gradient of Wnt activity that spans the PSM (Aulehla and Herrmann, 2004; Aulehla et al., 2003). By contrast, we conclude that Wnt regulates wavefront velocity in the posterior PSM, and this is temporally and spatially separated from the expression of segment determination markers and the arrest of oscillations. Our work therefore raises important questions about the mechanisms downstream of the Wnt activity gradient that transport and refine positional information.

We show that *spt* and *msgn1* are potential candidates for mediating the transfer of information from posterior Wnt signaling events towards the anterior in zebrafish. This list is almost certainly not exhaustive, and our studies do not address the mechanism by which these factors act upon the clock. Nevertheless, when combined with our estimates of the velocity of information propagation and the velocity of cell flow across the PSM, our findings lead us to a new model for how Wnt regulates the wavefront. In this scenario, Wnt provides positional information in the posterior that is transported by cell flow to determine segmental pattern and arrest cellular oscillations in the anterior, with a delay of several somite cycles. In other words, the falling level of Wnt starts an intracellular timer, or countdown, in posterior PSM cells that regulates when these cells will eventually switch off PSM behavior.

Strong evidence has accumulated that Wnt activity is required for the expression of transcriptional activators Tbx6 and Msgn1 in the mouse PSM, which are in turn required for expression in the anterior PSM of transcription factors vital for segment determination, such as Mesp2 and Ripply (Chalamalasetty et al., 2011; Dunty et al., 2008; Galceran et al., 2004; Hofmann et al., 2004; Wittler et al., 2007; Yasuhiko et al., 2006). However, this work did not examine where and when in the PSM Wnt activity is required, nor did it consider the consequences of cell flow through the tissue for wavefront regulation. Recent work in zebrafish has revealed striking roles for *spt* and *msgn1* in the differentiation and movement of mesoderm progenitor cells from the tailbud into the PSM, thereby contributing to the flow of cells through the tissue (Fior et al., 2012; Yabe and Takada, 2012). Following *msgn1* morpholino knockdown, Fior and colleagues reported the formation of smaller somites, whereas we observe larger somites in our assay. This apparent

Development (2014) doi:10.1242/dev.093435

discrepancy might arise from the different mechanisms involved in the long-term versus short-term effects of *msgn1* reduction and/or the level of reduction. To explain the shorter somites, the authors invoke a prolonged reduction of cell flow out of an enlarged tailbud (Fior et al., 2012), albeit without measurement of elongation or somitogenesis period or reference to wavefront velocity. This link between altered cell flow and somite length warrants further investigation. These studies also examined the role of *spt* and *msgn1* in the maturation of paraxial mesoderm, showing a cooperative activation of *tbx6* expression (Fior et al., 2012; Yabe and Takada, 2012). Tbx6 expression is a marker of mature PSM and is also an important transcriptional regulator of segment polarity (Nikaido et al., 2002). However, in these studies wavefront regulation was not considered. Our proposal explicitly joins the threads of a Wnt-initiated transcriptional cascade and cell flow through the PSM in the regulation of wavefront velocity.

This cell flow model for the regulation of wavefront velocity in zebrafish is consistent with scenarios explaining the distribution of posterior morphogen gradients along the mouse and chick embryonic axes by an mRNA or protein decay in a cell flow – the so-called 'gradient by inheritance' mechanism (Aulehla and Pourquié, 2010). Originally proposed as a mechanism to describe the graded distribution of Wingless signal away from the parasegment boundary in the *Drosophila* blastoderm (Pfeiffer et al., 2000), three examples have been described in vertebrates: the graded distribution of Cdx transcription factor as an input to Hox gene boundaries (Gaunt et al., 2003); a putative gradient of Wnt3a protein as an input into the direct concentration-threshold model of wavefront regulation (Aulehla et al., 2003); and the gradient of Fgf8 mRNA and protein, also involved in wavefront regulation (Dubrulle and Pourquié, 2004). The model suggested by our findings extends these scenarios because the information that is transported is not a single, decaying molecular species, but a regulatory cascade of components. This cascade downstream of Wnt signaling sets the wavefront position as it is transported with the cell flow. Segment length is determined by the velocity of this wavefront, which depends on the velocity of the cell flow as well as on the time scales of production, interaction and decay of the components in the downstream regulatory cascade.

Surgical manipulations in chick show that segments form rhythmically and sequentially even when the PSM is separated from the formed somites and tailbud (Palmeirim et al., 1998; Palmeirim et al., 1997), suggesting that the PSM has an autonomous schedule of wavefront progression. Furthermore, in grafts of entire chick PSM that are inverted along the A/P axis, the sequence of segment formation follows the pre-graft orientation of the PSM piece (Christ et al., 1974; Menkes and Sandor, 1969; Menkes et al., 1968; Palmeirim et al., 1998). Although the timing and lengths of the resulting segments were not measured in these experiments, this suggests that the schedule, once established, is relatively refractory to new input. The cell flow-based models above describe a mechanism consistent with these classical explant and inversion experiments. In the future, theoretical frameworks in which advection plays a prominent role will be essential for quantitative understanding of gradient formation and propagation of information in the PSM (Chisholm et al., 2010; Ibañes et al., 2006; Morelli et al., 2012).

Cross-talk with other signaling pathways may influence the positional information that PSM cells read from a given single gradient. Indeed, it is widely believed that cells are likely to integrate inputs from several gradients to determine wavefront position (Aulehla and Pourquié, 2010). Previous work in several species suggests that a gradient of Fgf signaling from the posterior and an opposing gradient of RA from the anterior regulate the wavefront (Dubrulle et al., 2001; Dubrulle and Pourquié, 2004; Moreno et al., 2008; Moreno and Kintner, 2004; Naiche et al., 2011; Sawada et al., 2001; Wahl et al., 2007). In mouse, strong gain and loss of β-catenin function in the PSM through conditional alleles causes an increase and decrease, respectively, in Fgf pathway gene expression (Aulehla et al., 2008; Dunty et al., 2008). In zebrafish, Fgf signaling appears to have a strong effect on wavefront positioning (Sawada et al., 2001), although the Fgf pathway does not appear to be a major downstream target of Wnt (Shimizu et al., 2005; Thorpe et al., 2005). Consistent with this, our results suggest that, for mild and time-controlled perturbation of Wnt signaling, the effects on the wavefront are not primarily dependent on alterations in Fgf signaling.

Using the distribution of dpErk, we have quantitated the Fgf signaling gradient in the PSM for the first time. In the tailbud, the Wnt and Fgf signaling gradients are oriented in different directions; whereas the Wnt gradient is flat or decreases monotonically towards the anterior, the Fgf signaling gradient rises from the posterior of the tailbud to a maximum level adjacent to the posterior end of the notochord. From this point, the orientation of the gradients is remarkably parallel, with Wnt and Fgf signaling reaching a minimum ~50-60% of the distance along the PSM. Therefore, neither gradient would be expected to trigger events via a concentration threshold in the anterior half of the PSM.

From the delayed response of Fgf signaling levels to Wnt reduction observed in our experiments, it seems likely that Fgf signaling is not simply a response to Wnt signaling in the zebrafish PSM. Rather, it is possible that cells receive parallel inputs from Wnt and Fgf signaling as they flow thorough the PSM. Wnt and RA have been proposed to regulate each other indirectly through Ntl in the tailbud (Martin and Kimelman, 2010; Martin and Kimelman, 2012), but the effects of RA on the wavefront in zebrafish remain unknown. Further studies will be required to address the integration of Wnt, Fgf and RA signaling in zebrafish segmentation and to identify the mechanisms that influence the precision of their positional information. Ultimately, the wavefront defines segment boundaries in cooperation with the clock, and this interaction will also influence the precision and interpretation of positional information. The approach we describe should help address how cells integrate these signals to define their position in the PSM.

Conclusions

In considering any pattern-forming system, mechanisms mediating the propagation of information can be weighed by the ratio of diffusion to advection of signals. The case of vertebrate segmentation is striking in that gradients of potentially diffusive signaling molecules act on a continuous flow of cellular oscillators that also transport the signals. It appears, at least for Wnt signaling, that the advective process of cell flow is dominant over diffusive processes in establishing and transporting positional information. In light of these properties, the segmentation clock is an important paradigm for developmental systems that use morphogen gradients. Our approach, in which we dissociate the dynamics of positional information from cell flow and segmentation clock period, might prove useful in investigating how positional information is provided, transported and refined to specify the future segment boundaries.

MATERIALS AND METHODS

Heat shock

hsaxin1::YFP (Kagermeier-Schenk et al., 2011), *hsdkk1::GFP* (Stoick-Cooper et al., 2007) or *hsWnt8::GFP* (Weidinger et al., 2005) transgenic

zebrafish were outcrossed with wild-type (WT) AB. Transgenic and WT siblings were simultaneously heat shocked for 30 minutes at 37°C. Somite number was recorded before heat shock (time 0). Multiple-embryo time-lapse microscopy was according to Herrgen et al. (Herrgen et al., 2009).

Measurements of *e*, *S*, T_s and *dL*/*dt*

Elongation velocity *e* was estimated from the distance of the tail tip to the posterior boundary of the fourth already-formed somite at the start of the movie. Instantaneous somite length *S* and somitogenesis period T_s were measured as described (Schröter et al., 2008). The rate of PSM shortening *dL*/*dt* was obtained from the distance between the last formed boundary and tail tip along the axis, each time a new somite formed. For *e*, T_s and *dL*/*dt*, slopes were calculated for each embryo and significance tested using Student's *t*-test, two-sided, unequal variance. For *S*, significance was determined by two-way ANOVA test with Bonferroni correction.

In situ hybridization and immunohistochemistry

To control for technical variation, control and transgenic embryos were processed in parallel, using identical procedures and reagents in a 24-well plate. Probe details are available in supplementary material Table S3. For immunohistochemistry, embryos were fixed in 2% (β-catenin) or 4% (dpErk) paraformaldehyde in 1×PBS at 4°C, washed in PBST (PBS with 0.1% Tween 20) and dehydrated overnight in methanol at −20°C. After progressive rehydration in PBST they were deyolked (β-catenin) and blocked in 10% sheep serum, 10 mg/ml BSA in PBS with 0.5% Triton X-100 (β-catenin) or 0.1% Tween 20 (dpErk). Anti-β-catenin antibody (Sigma, clone 15B8) was diluted 1/300 and goat anti-mouse IgG-coupled Alexa594 (Molecular Probes) and Hoechst 34222 were diluted 1/1000. Mouse monoclonal anti-dpErk [which recognizes Erk1/2 (Mapk3/1) in their double-phosphorylated state; gift of Ben Shilo, Weizmann Institute, Israel] was diluted 1/2000.

Image analysis

Distances between expression pattern and/or anatomical landmarks and expression profiles were measured on flat-mounted embryos. *myoD* (*myod1*), *axin2*, *ntl*, *spt* and *msgn1* expression profiles were generated using a segmented line of 40 pixel width on 8-bit RGB, color-inverted images using 'Analyze->Plot profile' in Fiji (Schindelin et al., 2012). To determine antibody staining intensity, the PSM was imaged with a 25× objective using confocal microscopy (Zeiss LSM 510) in several parts that were stitched together (Preibisch et al., 2009). For β-catenin, color channels were split, a nuclear mask was obtained with Cell Profiler software from the Hoechst signal and used to retrieve average intensity from the β-catenin signal. A corresponding position for each nucleus was determined using a custom Fiji plugin, which is available on request. Nuclear β-catenin intensity values were averaged for nuclei along the mediolateral axis with bins of 1.5% of PSM length (10 µm), using an R script. Intensity profiles from dpErk-immunostained embryos were obtained from grayscale images using a line of 50 pixel width, using 'Analyze->Plot profile' in Fiji. To reliably compare treatment effects, we averaged over multiple embryos. To determine the mid-point of graded distributions, we fitted a logarithmic response curve, for convenience, and calculated logEC50. To determine maximum intensity, we calculated dynamic range by subtracting the minimum from the maximum value for each embryo and normalizing to the average value of heat shocked WT embryos. Significance was assessed by multiple *t*-test.

Acknowledgements

We thank G. Weidinger and B. Kagermeier-Schenk for reagents and sharing preliminary results; M. Esner for R coding; L. Rohde, A. Webb, K. Uriu, G. Valentin, R. Desai, J. Briscoe and D. Kimelman for comments on the manuscript; S. Pralow, K. Straube and C. Fröb for technical support; and the fish and light microscopy facilities of the MPI-CBG.

Competing interests

The authors declare no competing financial interests.

Author contributions

L.B., L.G.M., S.A. and A.C.O. designed the experiments; L.B. performed the experiments; L.B., L.G.M., S.A., J.P. and F.J. analyzed the data; all authors wrote the manuscript.

Funding

This work was supported by the Max Planck Society; L.B. by Human Frontier Science Program (HFSP) and Marie Curie; A.C.O., L.G.M. and J.P. by the European Research Council (ERC) under the European Communities 7th Framework Programme [FP7/2007–2013]/[ERC grant 207634]; J.P. by German Research Foundation Normalverfaren [OA 53/2-1]; S.A. by Spanish Ministry of Economy and Competitiveness (MINECO) grant PHYSDEV [FIS2012-32349]; F.J. by the Max Planck Society; and A.C.O. by the Wellcome Trust [WT098025MA] and the Medical Research Council (MRC) [MC_UP_1202/3]. Deposited in PMC for immediate release.

Supplementary material

Supplementary material available online at
http://dev.biologists.org/lookup/suppl/doi:10.1242/dev.093435/-/DC1

References

Aulehla, A. and Herrmann, B. G. (2004). Segmentation in vertebrates: clock and gradient finally joined. *Genes Dev.* **18**, 2060-2067.
Aulehla, A. and Pourquié, O. (2010). Signaling gradients during paraxial mesoderm development. *Cold Spring Harb. Perspect. Biol.* **2**, a000869.
Aulehla, A., Wehrle, C., Brand-Saberi, B., Kemler, R., Gossler, A., Kanzler, B. and Herrmann, B. G. (2003). Wnt3a plays a major role in the segmentation clock controlling somitogenesis. *Dev. Cell* **4**, 395-406.
Aulehla, A., Wiegraebe, W., Baubet, V., Wahl, M. B., Deng, C., Taketo, M., Lewandoski, M. and Pourquié, O. (2008). A beta-catenin gradient links the clock and wavefront systems in mouse embryo segmentation. *Nat. Cell Biol.* **10**, 186-193.
Buchberger, A., Bonneick, S. and Arnold, H. (2000). Expression of the novel basic-helix-loop-helix transcription factor cMespo in presomitic mesoderm of chicken embryos. *Mech. Dev.* **97**, 223-226.
Chalamalasetty, R. B., Dunty, W. C., Jr, Biris, K. K., Ajima, R., Iacovino, M., Beisaw, A., Feigenbaum, L., Chapman, D. L., Yoon, J. K., Kyba, M. et al. (2011). The Wnt3a/β-catenin target gene Mesogenin1 controls the segmentation clock by activating a Notch signalling program. *Nat. Commun.* **2**, 390.
Chen, H., Xu, Z., Mei, C., Yu, D. and Small, S. (2012). A system of repressor gradients spatially organizes the boundaries of Bicoid-dependent target genes. *Cell* **149**, 618-629.
Chien, A. J., Conrad, W. H. and Moon, R. T. (2009). A Wnt survival guide: from flies to human disease. *J. Invest. Dermatol.* **129**, 1614-1627.
Chisholm, R. H., Hughes, B. D. and Landman, K. A. (2010). Building a morphogen gradient without diffusion in a growing tissue. *PLoS ONE* **5**, e12857.
Christ, B., Jacob, H. J. and Jacob, M. (1974). Somitogenesis in the chick embryo. Determination of the segmentation direction. *Verh. Anat. Ges.* **68**, 573-579.
Cooke, J. and Zeeman, E. C. (1976). A clock and wavefront model for control of the number of repeated structures during animal morphogenesis. *J. Theor. Biol.* **58**, 455-476.
Dahmann, C., Oates, A. C. and Brand, M. (2011). Boundary formation and maintenance in tissue development. *Nat. Rev. Genet.* **12**, 43-55.
Delaune, E. A., François, P., Shih, N. P. and Amacher, S. L. (2012). Single-cell-resolution imaging of the impact of Notch signaling and mitosis on segmentation clock dynamics. *Dev. Cell* **23**, 995-1005.
Dubrulle, J. and Pourquié, O. (2004). fgf8 mRNA decay establishes a gradient that couples axial elongation to patterning in the vertebrate embryo. *Nature* **427**, 419-422.
Dubrulle, J., McGrew, M. J. and Pourquié, O. (2001). FGF signaling controls somite boundary position and regulates segmentation clock control of spatiotemporal Hox gene activation. *Cell* **106**, 219-232.
Dunty, W. C., Jr, Biris, K. K., Chalamalasetty, R. B., Taketo, M. M., Lewandoski, M. and Yamaguchi, T. P. (2008). Wnt3a/beta-catenin signaling controls posterior body development by coordinating mesoderm formation and segmentation. *Development* **135**, 85-94.
Fior, R., Maxwell, A. A., Ma, T. P., Vezzaro, A., Moens, C. B., Amacher, S. L., Lewis, J. and Saúde, L. (2012). The differentiation and movement of presomitic mesoderm progenitor cells are controlled by Mesogenin 1. *Development* **139**, 4656-4665.
Galceran, J., Sustmann, C., Hsu, S. C., Folberth, S. and Grosschedl, R. (2004). LEF1-mediated regulation of Delta-like1 links Wnt and Notch signaling in somitogenesis. *Genes Dev.* **18**, 2718-2723.
Gaunt, S. J., Drage, D. and Cockley, A. (2003). Vertebrate caudal gene expression gradients investigated by use of chick cdx-A/lacZ and mouse cdx-1/lacZ reporters in transgenic mouse embryos: evidence for an intron enhancer. *Mech. Dev.* **120**, 573-586.
Gibb, S., Zagorska, A., Melton, K., Tenin, G., Vacca, I., Trainor, P., Maroto, M. and Dale, J. K. (2009). Interfering with Wnt signalling alters the periodicity of the segmentation clock. *Dev. Biol.* **330**, 21-31.
Gomez, C., Ozbudak, E. M., Wunderlich, J., Baumann, D., Lewis, J. and Pourquié, O. (2008). Control of segment number in vertebrate embryos. *Nature* **454**, 335-339.
Greco, T. L., Takada, S., Newhouse, M. M., McMahon, J. A., McMahon, A. P. and Camper, S. A. (1996). Analysis of the vestigial tail mutation demonstrates that Wnt-3a gene dosage regulates mouse axial development. *Genes Dev.* **10**, 313-324.
Groves, J. A., Hammond, C. L. and Hughes, S. M. (2005). Fgf8 drives myogenic progression of a novel lateral fast muscle fibre population in zebrafish. *Development* **132**, 4211-4222.
Harima, Y., Takashima, Y., Ueda, Y., Ohtsuka, T., and Kageyama, R. (2013). Accelerating the tempo of the segmentation clock by reducing the number of introns in the Hes7 gene. *Cell Rep.* **3**, 1-7.

Herrgen, L., Schröter, C., Bajard, L. and Oates, A. C. (2009). Multiple embryo time-lapse imaging of zebrafish development. *Methods Mol. Biol.* **546**, 243-254.
Herrgen, L., Ares, S., Morelli, L. G., Schroter, C., Julicher, F., and Oates, A. C. (2010). Intercellular coupling regulates the period of the segmentation clock. *Curr. Biol.* **20**, 1244-1253.
Hofmann, M., Schuster-Gossler, K., Watabe-Rudolph, M., Aulehla, A., Herrmann, B. G. and Gossler, A. (2004). WNT signaling, in synergy with T/TBX6, controls Notch signaling by regulating Dll1 expression in the presomitic mesoderm of mouse embryos. *Genes Dev.* **18**, 2712-2717.
Holley, S. A., Geisler, R. and Nüsslein-Volhard, C. (2000). Control of her1 expression during zebrafish somitogenesis by a delta-dependent oscillator and an independent wave-front activity. *Genes Dev.* **14**, 1678-1690.
Ibañes, M., Kawakami, Y., Rasskin-Gutman, D. and Izpisúa Belmonte, J. C. (2006). Cell lineage transport: a mechanism for molecular gradient formation. *Mol. Syst. Biol.* **2**, 57.
Jho, E. H., Zhang, T., Domon, C., Joo, C. K., Freund, J. N. and Costantini, F. (2002). Wnt/beta-catenin/Tcf signaling induces the transcription of Axin2, a negative regulator of the signaling pathway. *Mol. Cell. Biol.* **22**, 1172-1183.
Kagermeier-Schenk, B., Wehner, D., Ozhan-Kizil, G., Yamamoto, H., Li, J., Kirchner, K., Hoffmann, C., Stern, P., Kikuchi, A., Schambony, A. et al. (2011). Waif1/5T4 inhibits Wnt/β-catenin signaling and activates noncanonical Wnt pathways by modifying LRP6 subcellular localization. *Dev. Cell* **21**, 1129-1143.
Kelly, G. M., Greenstein, P., Erezyilmaz, D. F. and Moon, R. T. (1995). Zebrafish wnt8 and wnt8b share a common activity but are involved in distinct developmental pathways. *Development* **121**, 1787-1799.
Lekven, A. C., Thorpe, C. J., Waxman, J. S. and Moon, R. T. (2001). Zebrafish wnt8 encodes two wnt8 proteins on a bicistronic transcript and is required for mesoderm and neurectoderm patterning. *Dev. Cell* **1**, 103-114.
Martin, B. L., and Kimelman, D. (2009). Wnt signaling and the evolution of embryonic posterior development. *Curr. Biol.* **19**, R215-R219.
Martin, B. L. and Kimelman, D. (2010). Brachyury establishes the embryonic mesodermal progenitor niche. *Genes Dev.* **24**, 2778-2783.
Martin, B. L. and Kimelman, D. (2012). Canonical Wnt signaling dynamically controls multiple stem cell fate decisions during vertebrate body formation. *Dev. Cell* **22**, 223-232.
Masamizu, Y., Ohtsuka, T., Takashima, Y., Nagahara, H., Takenaka, Y., Yoshikawa, K., Okamura, H. and Kageyama, R. (2006). Real-time imaging of the somite segmentation clock: revelation of unstable oscillators in the individual presomitic mesoderm cells. *Proc. Natl. Acad. Sci. USA* **103**, 1313-1318.
Menkes, B. and Sandor, S. (1969). Researches on the formation of axial organs of the chick embryo. V. *Revue Roumaine d'Embryologie et de Cytologie* **6**, 65-77.
Menkes, B., Sandor, S. and Elias, S. (1968). Researches on the formation of axial organs of the chick embryo. IV. *Revue Roumaine d'Embryologie et de Cytologie* **5**, 131-137.
Morelli, L. G., Ares, S., Herrgen, L., Schröter, C., Jülicher, F. and Oates, A. C. (2009). Delayed coupling theory of vertebrate segmentation. *HFSP J.* **3**, 55-66.
Morelli, L. G., Uriu, K., Ares, S. and Oates, A. C. (2012). Computational approaches to developmental patterning. *Science* **336**, 187-191.
Moreno, T. A. and Kintner, C. (2004). Regulation of segmental patterning by retinoic acid signaling during Xenopus somitogenesis. *Dev. Cell* **6**, 205-218.
Moreno, T. A., Jappelli, R., Izpisúa Belmonte, J. C. and Kintner, C. (2008). Retinoic acid regulation of the Mesp-Ripply feedback loop during vertebrate segmental patterning. *Dev. Biol.* **315**, 317-330.
Murray, P. J., Maini, P. K. and Baker, R. E. (2011). The clock and wavefront model revisited. *J. Theor. Biol.* **283**, 227-238.
Naiche, L. A., Holder, N. and Lewandoski, M. (2011). FGF4 and FGF8 comprise the wavefront activity that controls somitogenesis. *Proc. Natl. Acad. Sci. USA* **108**, 4018-4023.
Nikaido, M., Kawakami, A., Sawada, A., Furutani-Seiki, M., Takeda, H. and Araki, K. (2002). Tbx24, encoding a T-box protein, is mutated in the zebrafish somite-segmentation mutant fused somites. *Nat. Genet.* **31**, 195-199.
Oates, A. C., Rohde, L. A. and Ho, R. K. (2005). Generation of segment polarity in the paraxial mesoderm of the zebrafish through a T-box-dependent inductive event. *Dev. Biol.* **283**, 204-214.
Oates, A. C., Morelli, L. G. and Ares, S. (2012). Patterning embryos with oscillations: structure, function and dynamics of the vertebrate segmentation clock. *Development* **139**, 625-639.
Palmeirim, I., Henrique, D., Ish-Horowicz, D. and Pourquié, O. (1997). Avian hairy gene expression identifies a molecular clock linked to vertebrate segmentation and somitogenesis. *Cell* **91**, 639-648.
Palmeirim, I., Dubrulle, J., Henrique, D., Ish-Horowicz, D. and Pourquié, O. (1998). Uncoupling segmentation and somitogenesis in the chick presomitic mesoderm. *Dev. Genet.* **23**, 77-85.
Pfeiffer, S., Alexandre, C., Calleja, M., and Vincent, J. P. (2000). The progeny of wingless-expressing cells deliver the signal at a distance in Drosophila embryos. *Curr. Biol.* **10**, 321-324.
Picker, A., Cavodeassi, F., Machate, A., Bernauer, S., Hans, S., Abe, G., Kawakami, K., Wilson, S. W. and Brand, M. (2009). Dynamic coupling of pattern formation and morphogenesis in the developing vertebrate retina. *PLoS Biol.* **7**, e1000214.
Porcher, A., and Dostatni, N. (2010). The bicoid morphogen system. *Curr. Biol.* **20**, R249-R254.
Pourquié, O. (2011). Vertebrate segmentation: from cyclic gene networks to scoliosis. *Cell* **145**, 650-663.
Pourquié, O. and Tam, P. P. (2001). A nomenclature for prospective somites and phases of cyclic gene expression in the presomitic mesoderm. *Dev. Cell* **1**, 619-620.
Preibisch, S., Saalfeld, S. and Tomancak, P. (2009). Globally optimal stitching of tiled 3D microscopic image acquisitions. *Bioinformatics* **25**, 1463-1465.
Rogers, K. W. and Schier, A. F. (2011). Morphogen gradients: from generation to interpretation. *Annu. Rev. Cell Dev. Biol.* **27**, 377-407.
Row, R. H. and Kimelman, D. (2009). Bmp inhibition is necessary for post-gastrulation patterning and morphogenesis of the zebrafish tailbud. *Dev. Biol.* **329**, 55-63.
Saga, Y., Hata, N., Koseki, H. and Taketo, M. M. (1997). Mesp2: a novel mouse gene expressed in the presegmented mesoderm and essential for segmentation initiation. *Genes Dev.* **11**, 1827-1839.
Sawada, A., Fritz, A., Jiang, Y. J., Yamamoto, A., Yamasu, K., Kuroiwa, A., Saga, Y. and Takeda, H. (2000). Zebrafish Mesp family genes, mesp-a and mesp-b are segmentally expressed in the presomitic mesoderm, and Mesp-b confers the anterior identity to the developing somites. *Development* **127**, 1691-1702.
Sawada, A., Shinya, M., Jiang, Y. J., Kawakami, A., Kuroiwa, A. and Takeda, H. (2001). Fgf/MAPK signalling is a crucial positional cue in somite boundary formation. *Development* **128**, 4873-4880.
Schindelin, J., Arganda-Carreras, I., Frise, E., Kaynig, V., Longair, M., Pietzsch, T., Preibisch, S., Rueden, C., Saalfeld, S., Schmid, B. et al. (2012). Fiji: an open-source platform for biological-image analysis. *Nat. Methods* **9**, 676-682.
Schroter, C., and Oates, A. C. (2010). Segment number and axial identity in a segmentation clock period mutant. *Curr. Biol.* **20**, 1254-1258.
Schröter, C., Herrgen, L., Cardona, A., Brouhard, G. J., Feldman, B. and Oates, A. C. (2008). Dynamics of zebrafish somitogenesis. *Dev. Dyn.* **237**, 545-553.
Shimizu, T., Bae, Y. K., Muraoka, O. and Hibi, M. (2005). Interaction of Wnt and caudal-related genes in zebrafish posterior body formation. *Dev. Biol.* **279**, 125-141.
Stoick-Cooper, C. L., Weidinger, G., Riehle, K. J., Hubbert, C., Major, M. B., Fausto, N. and Moon, R. T. (2007). Distinct Wnt signaling pathways have opposing roles in appendage regeneration. *Development* **134**, 479-489.
Stulberg, M. J., Lin, A., Zhao, H. and Holley, S. A. (2012). Crosstalk between Fgf and Wnt signaling in the zebrafish tailbud. *Dev. Biol.* **369**, 298-307.
Szeto, D. P. and Kimelman, D. (2004). Combinatorial gene regulation by Bmp and Wnt in zebrafish posterior mesoderm formation. *Development* **131**, 3751-3760.
Thorpe, C. J., Weidinger, G. and Moon, R. T. (2005). Wnt/beta-catenin regulation of the Sp1-related transcription factor sp5l promotes tail development in zebrafish. *Development* **132**, 1763-1772.
van Eeden, F. J., Granato, M., Schach, U., Brand, M., Furutani-Seiki, M., Haffter, P., Hammerschmidt, M., Heisenberg, C. P., Jiang, Y. J., Kane, D. A. et al. (1996). Mutations affecting somite formation and patterning in the zebrafish, Danio rerio. *Development* **123**, 153-164.
Wahl, M. B., Deng, C., Lewandoski, M. and Pourquié, O. (2007). FGF signaling acts upstream of the NOTCH and WNT signaling pathways to control segmentation clock oscillations in mouse somitogenesis. *Development* **134**, 4033-4041.
Weidinger, G., Thorpe, C. J., Wuennenberg-Stapleton, K., Ngai, J., and Moon, R. T. (2005). The Sp1-related transcription factors sp5 and sp5-like act downstream of Wnt/beta-catenin signaling in mesoderm and neuroectoderm patterning. *Curr. Biol.* **15**, 489-500.
Wilson, V., Olivera-Martinez, I. and Storey, K. G. (2009). Stem cells, signals and vertebrate body axis extension. *Development* **136**, 1591-1604.
Wittler, L., Shin, E. H., Grote, P., Kispert, A., Beckers, A., Gossler, A., Werber, M. and Herrmann, B. G. (2007). Expression of Msgn1 in the presomitic mesoderm is controlled by synergism of WNT signalling and Tbx6. *EMBO Rep.* **8**, 784-789.
Yabe, T. and Takada, S. (2012). Mesogenin causes embryonic mesoderm progenitors to differentiate during development of zebrafish tail somites. *Dev. Biol.* **370**, 213-222.
Yasuhiko, Y., Haraguchi, S., Kitajima, S., Takahashi, Y., Kanno, J. and Saga, Y. (2006). Tbx6-mediated Notch signaling controls somite-specific Mesp2 expression. *Proc. Natl. Acad. Sci. USA* **103**, 3651-3656.
Yu, S. R., Burkhardt, M., Nowak, M., Ries, J., Petrásek, Z., Scholpp, S., Schwille, P. and Brand, M. (2009). Fgf8 morphogen gradient forms by a source-sink mechanism with freely diffusing molecules. *Nature* **461**, 533-536.

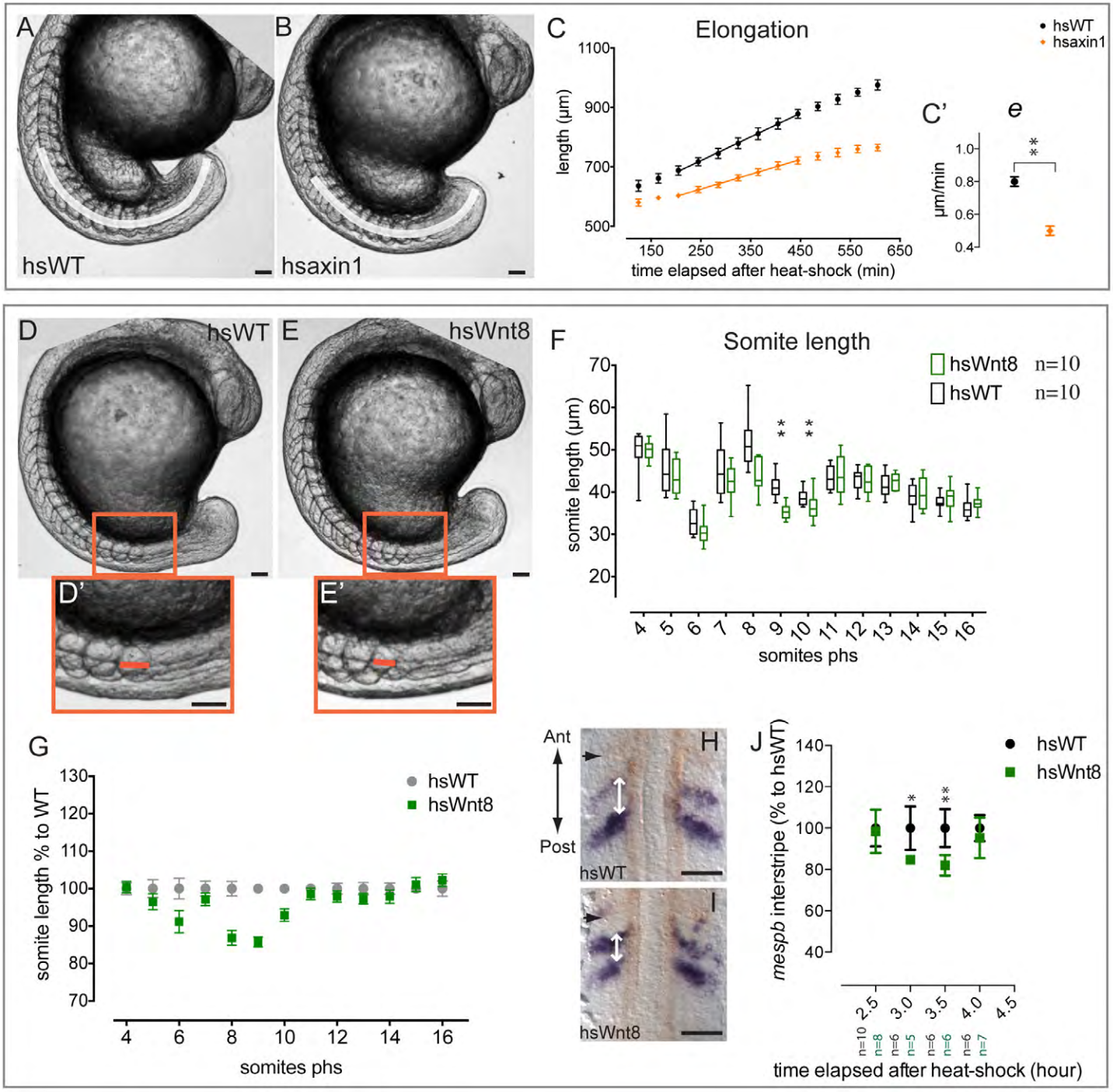

Figure S1. Effect of expression of *hsaxin1* on elongation and of *hsWnt8* on somite length, related to Figure 1.
(A-C') *hsaxin1::YFP* heterozygote outcross. (D-J) *hsWnt8::GFP* heterozygote outcross. (A,B,D,E) Lateral view of representative control (A,D) or transgenic (B,E) embryo when the 9th somite (A,B) or 10th somite (D,E) after the heat-shock is forming. (D',E') Close-up of the 3 last formed somites. (C) Mean ± SD of distance between a fixed position in the somites and the posterior tip of the embryo (white line in A,B) over time. (C') Slope of the linear fit indicated in C. (F) Box plot of somite length (distance between two consecutive notches, orange line in D',E') measured from an experiment in which the heat-shock was performed at 6 somites ; n=10 per condition. (G) Normalized mean somite length ± SEM measured from 4 experiments. (H,I) Dorsal view of the anterior PSM of control (H) or transgenic (I) embryos double stained for *mespb* (blue) and *MyoD* (red), fixed 3.5 h (~7 somites) after heat-shock. (J) Mean ± SD of segment length, the distance between the anterior margins of two *mespb* stripes measured as indicated with white arrows in H, I, on embryos fixed at successive time points after heat-shock. * p<0.01, ** p<0.001

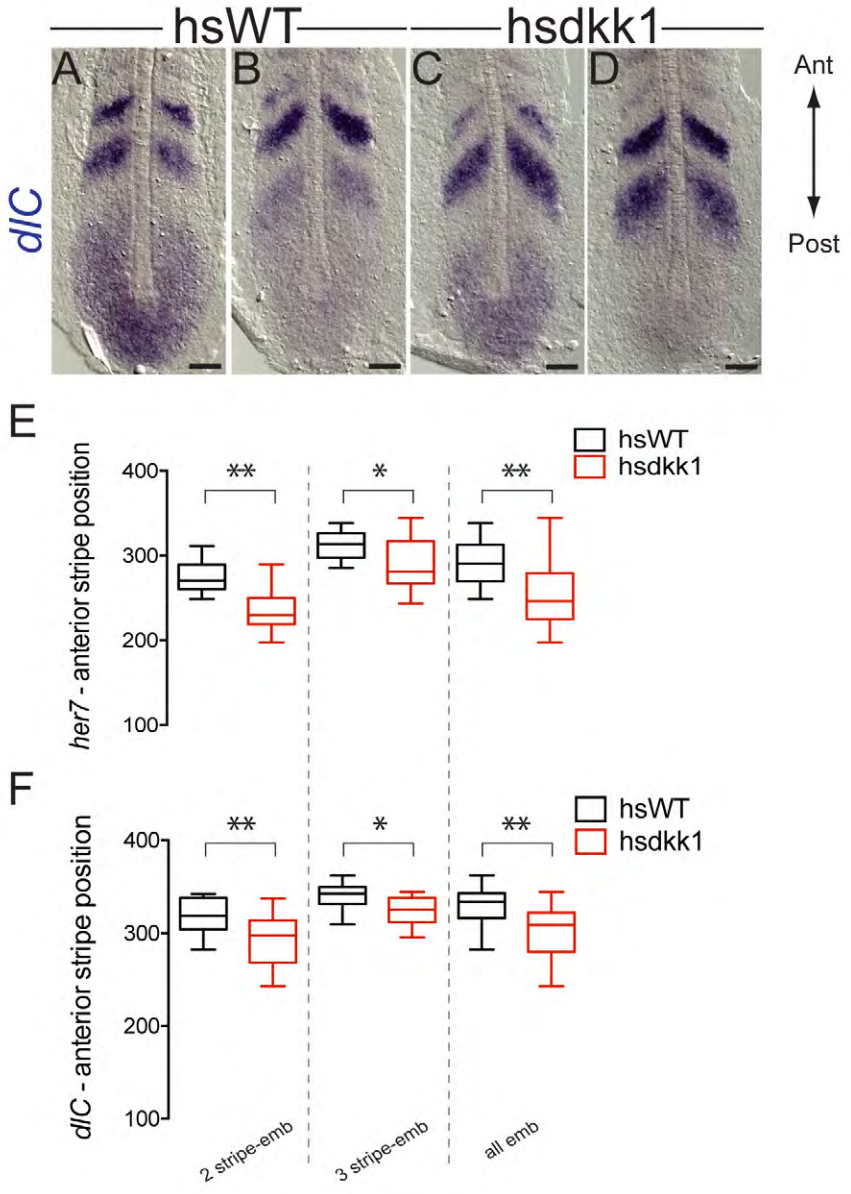

Figure S2. Effect of Wnt inhibition on *dlC* and *her7* expression at ~7 somites phs, related to Figure 3.
(A-D) Dorsal views of flat-mounted PSM from *hsdkk1::*GFP (C,D) or their WT siblings (A,B) heat-shocked at 2 somites, fixed 3.5 h phs and stained for *dlC*. (E,F) Box Plot of the distance between anterior-most stripe of *her7* (E) or *dlC* (F) and the posterior end of the notochord measured from embryos displaying 2 stripes or 3 stripes or both. * $p<0.01$, ** $p<0.001$. Scale bar 50µm.

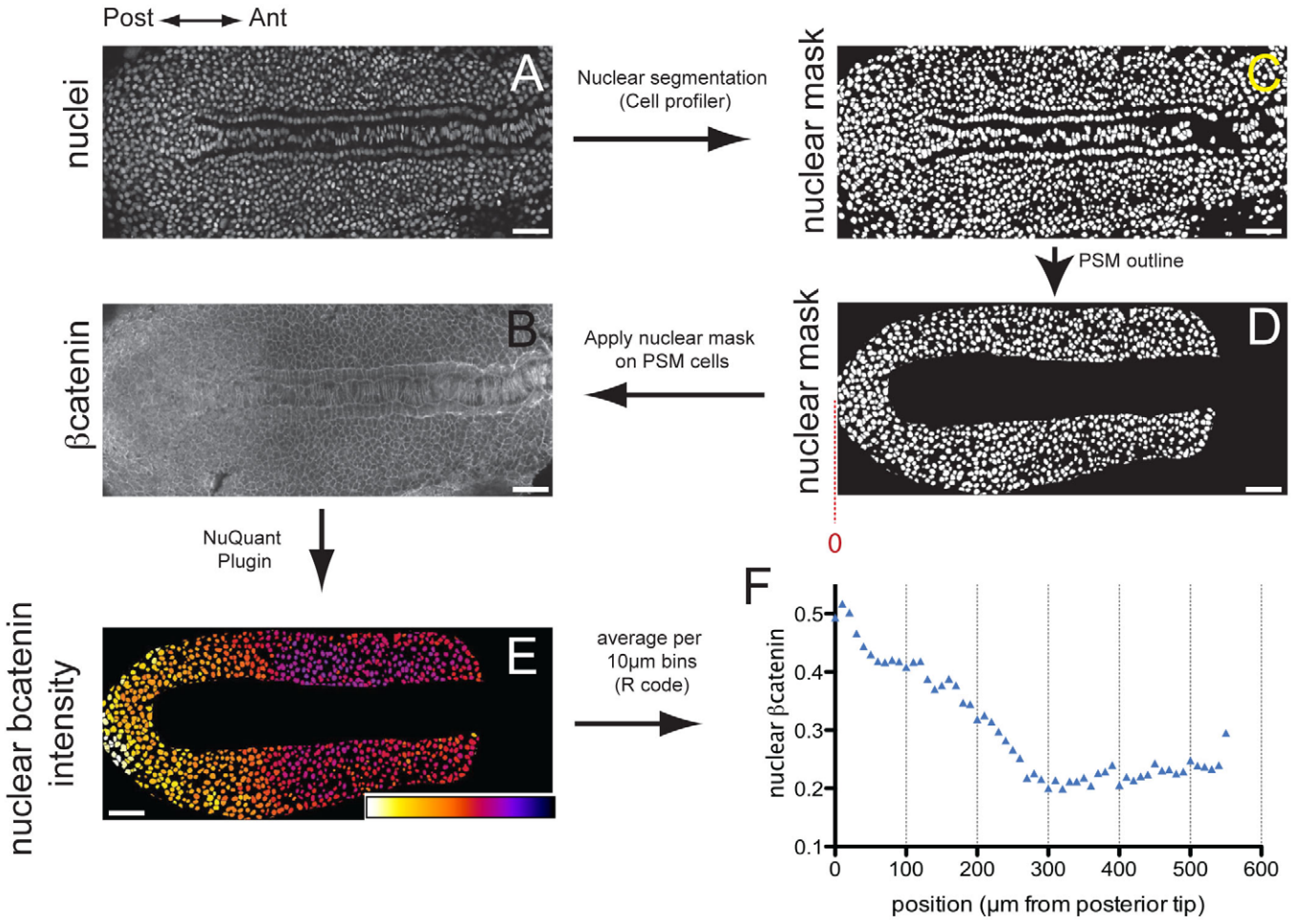

Figure S3. Procedure for measuring fluorescence intensity of nuclear βcatenin staining, related to Figure 4.
(A-E) Dorsal view of the flat mounted PSM of a 10 somite stage embryo. (A,B) Raw images of Hoechst 34222 nuclear staining (A) and βcatenin immunostaining (B). (C-E) Processed images showing nuclear mask obtained from Hoechst staining after nuclear segmentation (C), nuclei in the PSM area, which is outlined manually (D) and fluorescence intensity of nuclear βcatenin staining in PSM cells after applying a nuclear mask, displayed using false color. White is high and blue is low (E). (F) Intensity of nuclear βcatenin staining for one embryo averaged within bins of 10 μm and plotted along the antero-posterior length of the PSM.

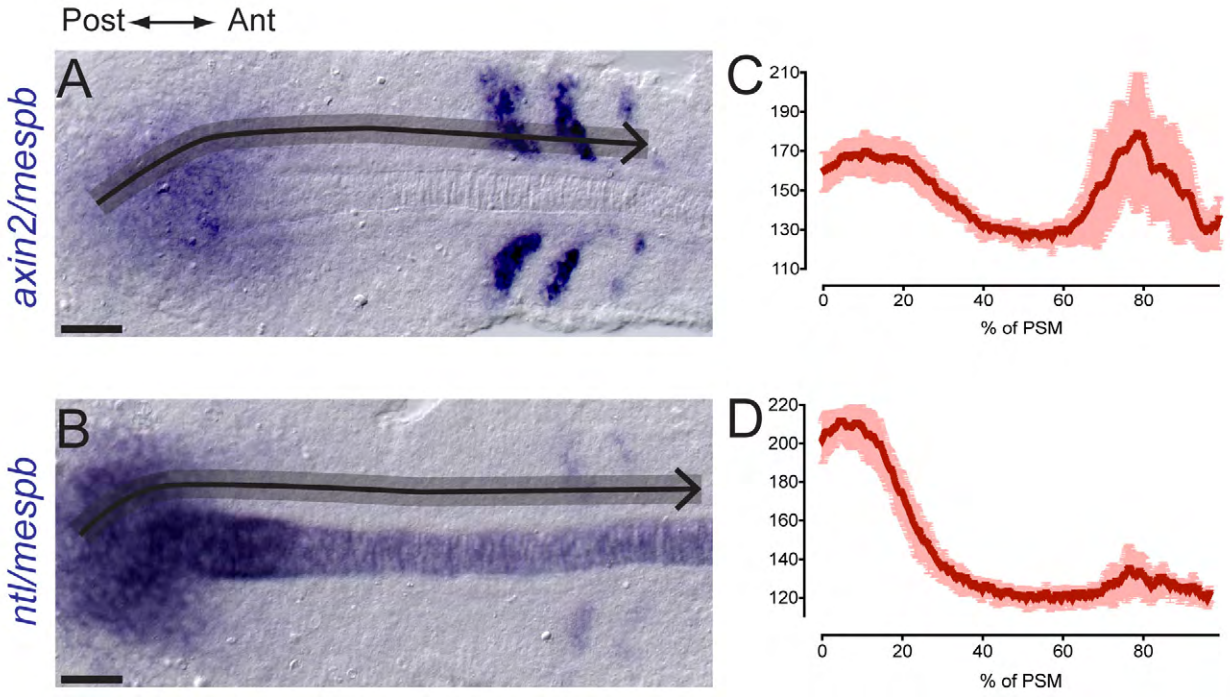

Figure S4. Intensity profiles of *axin2* and *notail* (*ntl*) along normalized antero-posterior PSM length, related to Figure 4. (A,B) Dorsal view of flat mounted PSM of wild-type embryos at 12 (A) or 10 (B) somites, stained for *axin2* and *mespb* (A) or *ntl* and *mespb* (B). (C,D) Average intensity profiles from several embryos obtained from color-inverted pictures, within a line of interest that spans the PSM (see black arrows in A and B). The grey shading indicates the width of the Line of Interest used for measurements. Mean ± SD. Scale bar is 50µm.

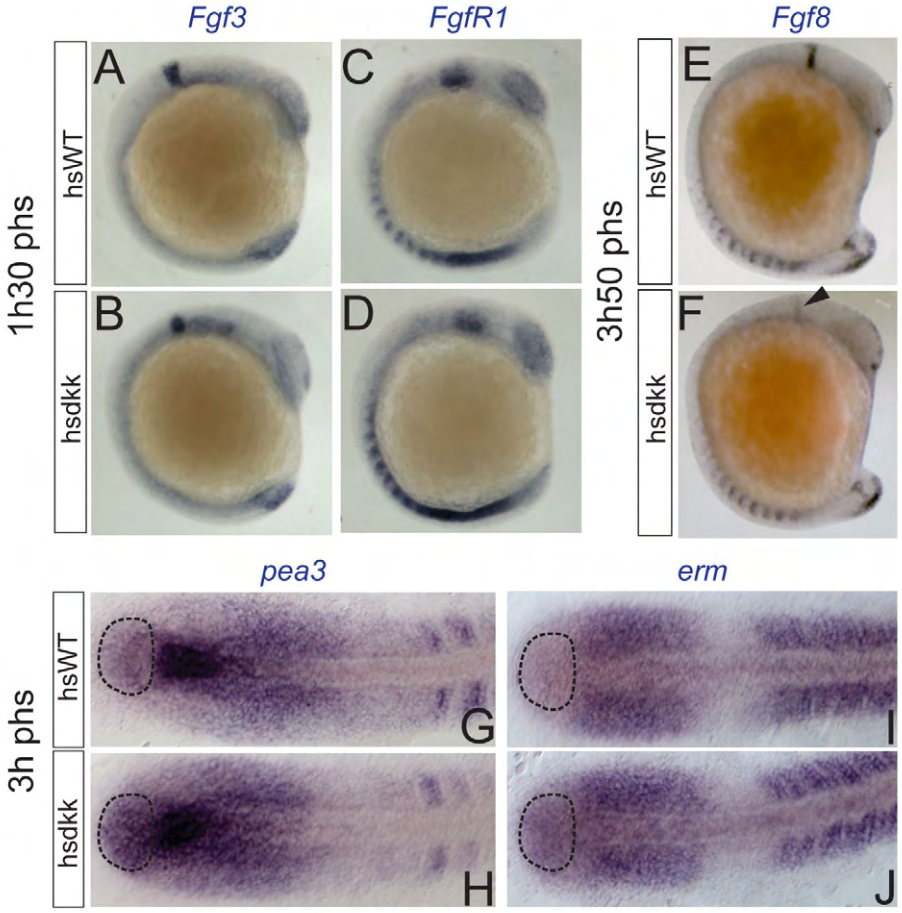

Figure S5. Expression of Fgf pathway members after Dkk overexpression, related to Figure 5.
(A-F) Lateral view of *hsdkk1::*GFP (B,D,F) embryos or WT siblings (A,C,E) heat-shocked at 8 (A-D) or 6 (E,F) somites, fixed 1.5 h (A-D) or 3.8 h (E,F) phs and hybridized with *fgf3* (A,B), *fgfr1* (C,D) or *fgf8* (E,F) probes. Arrowhead shows domain of reduced *fgf8* expression in mid-hindbrain boundary. (G-J) Dorsal view of flat mounted PSM of *hsdkk1::*GFP (H,J) or WT siblings (G,I) heat-shocked at 8 somites, fixed 3 h phs and hybridized with *pea3* (G,H) or *erm* (I,J) probes. Dashed outline indicates domain of expression elevated in *hsdkk1* embryos.

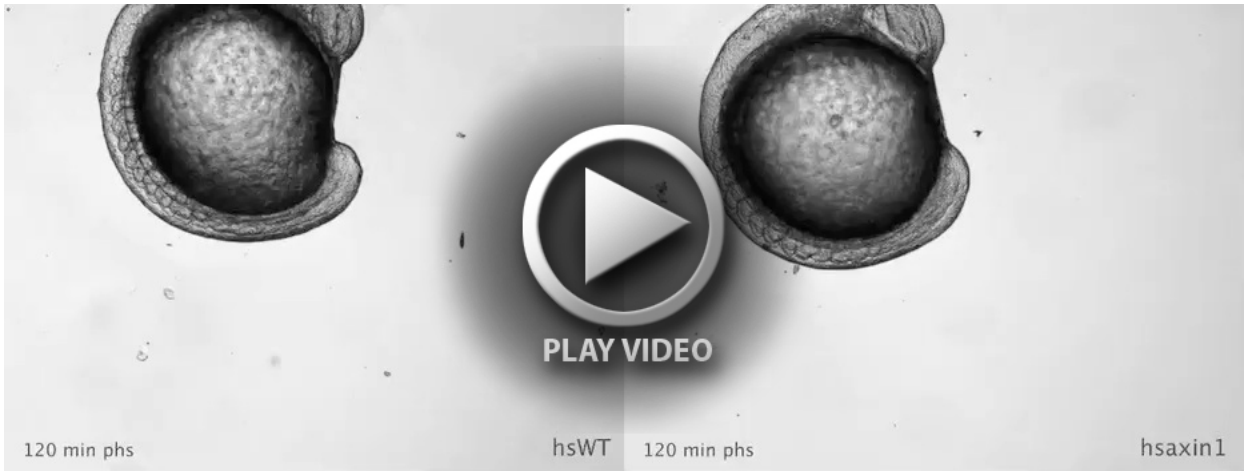

Movie 1. Effects of time-controlled Axin1 overexpression on trunk somitogenesis and elongation, related to Figure 1. Bright-field time-lapse movies of hsWT and hsaxin1 embryos corresponding to Figure S1A,B. Embryos from *hsaxin1::YFP*/+ outcross to a wildtype AB are recorded in parallel, with a 5 minute interval between successive time frames. Embryos were heat-shocked at ~9 somites and imaged 120 minutes (~4 somites) later.

Movie 2. Effects of time-controlled Dkk1 overexpression on trunk somitogenesis and elongation, related to Figure 1. Bright-field time-lapse movies of hsWT and hsdkk1 embryos corresponding to Figure 1A,B,A',B' in the main text. Embryos from *hsdkk1::GFP*/+ outcross to a wildtype AB are recorded in parallel, with a 4 minute interval between successive time frames. Embryos were heat-shocked at ~9 somites and imaged 80 minutes (~3 somites) later.

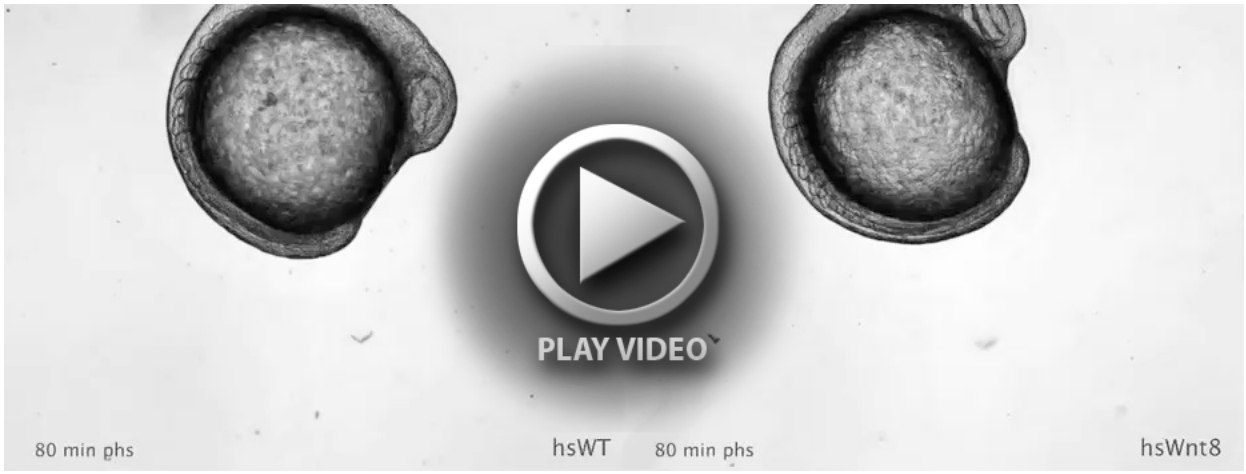

Movie 3. Effects of time-controlled Wnt8 overexpression on trunk somitogenesis and elongation, related to Figure 1. Bright-field time-lapse movies of hsWT and hsWnt8 corresponding to Figure S1D,E,D',E'. Embryos from *hsWnt8::GFP*/+ outcross to a wildtype AB are recorded in parallel, with a 5 minute interval between successive time frames. Embryos were heat-shocked at ~6 somites and imaged 80 minutes (~3 somites) later.

Interval and parameter		Genotype	Stage at heatshock: 1 somite		2 somites	7 somites		9 somites	
7th - 13th som phs	***e*** (µm/min)	hsWT	1.12 ± 0.15	1.11 ± 0.06	1.04 ± 0.08	0.81 ± 0.06	0.68 ± 0.06	0.78 ± 0.06	0.84 ± 0.05
		hsdkk	1.08 ± 0.16	**0.97 ± 0.08 *↓**	1.03 ± 0.14	0.80 ± 0.07	**0.78 ± 0.05 *↑**	0.79 ± 0.06	0.87 ± 0.08
	-dL/dt (µm/min)	hsWT	0.58 ± 0.15	0.57 ± 0.18	0.77 ± 0.09	0.72 ± 0.14	0.68 ± 0.07	0.45 ± 0.04	0.43 ± 0.06
		hsdkk	**1.23 ± 0.15 **↑**	**1.30 ± 0.30 **↑**	**1.16 ± 0.13 **↑**	**0.93 ± 0.11 *↑**	0.71 ± 0.13	**0.65 ± 0.12 **↑**	**0.60 ± 0.08 **↑**
	Ts (min)	hsWT	27.1 ± 0.8	29.2 ± 2.3	29.6 ± 1.0	30.7 ± 3.1	32.8 ± 1.6	34.1 ± 1.1	34.5 ± 2.1
		hsdkk	26.6 ± 2.0	30.0 ± 2.5	29.6 ± 1.0	33.1 ± 1.7	**34.6 ± 1.6 *↑**	36.6 ± 2.4	36.3 ± 2.2
12-17th som phs	***e*** (µm/min)	hsWT	1.0 ± 0.1	0.82 ± 0.05	0.70 ± 0.06	ND		ND	
		hsdkk	**0.85 ± 0.12 *↓**	**0.73 ± 0.07 *↓**	**0.60 ± 0.03 *↓**				

Table S1: Elongation velocity (*e*), PSM shortening (-*dL*/*dt*), and Somitogenesis period (*Ts*), related to Figures 1 and 2.

Heat-shock was performed at 1, 2, 7, or 9 somite stages on either wildtype (WT) or hsp70:dkk1 transgenic (hsdkk) embryos. Results of 2 replicate experiments are shown for heat-shock at 1, 7, or 9 somite stages. The experiment shown in Figure 1A-D and Figure 2A,A',C,C' is highlighted in yellow. Mean ± SD, 6≤n≤8 embryos per condition for each experiment. Significant differences (Student T-test, two-sided, unequal variance) are indicated in bold, * $p<0.05$, ** $p\leq0.001$, with direction of change indicated by arrow. som phs, somites post-heatshock.

Method of inference	Genotype	Stage at heatshock: 1 somite		2 somites	7 somites		9 somites	
$v_m = e - dL/dt$ (μm/min)	hsWT	1.70 ± 0.07	1.68 ± 0.17	1.70 ± 0.10	1.53 ± 0.15	1.36 ± 0.04	1.23 ± 0.07	1.27 ± 0.07
	hsdkk	**2.31 ± 0.08 **↑**	**2.27 ± 0.30 **↑**	**2.05 ± 0.09 **↑**	**1.73 ± 0.11 *↑**	**1.49 ± 0.1 *↑**	**1.44 ± 0.11 **↑**	**1.47 ± 0.14 *↑**
$v_m = S/Ts$ (μm/min)	hsWT	1.78 ± 0.09	1.63 ± 0.12	1.69 ± 0.11	1.66 ± 0.13	1.32 ± 0.09	1.12 ± 0.07	1.12 ± 0.06
	hsdkk	**2.32 ± 0.17 **↑**	**1.96 ± 0.16 **↑**	**1.97 ± 0.07 **↑**	1.76 ± 0.13	**1.47 ± 0.1 *↑**	**1.33 ± 0.09 **↑**	**1.30 ± 0.1 *↑**

Table S2: Inference of morphological wavefront regression velocity (v_m) using measurements from bright field time-lapse movies, related to Figure 2. Heat-shock was performed at 1, 2, 7 or 9 somite stages on either wildtype (WT) or hsp70:dkk1 transgenic (hsdkk) embryos. Results from 7 independent experiments are shown. Values corresponding to the experiment shown in Figure 2D are highlighted in yellow. Significant differences (Student T-test, two-sided, unequal variance) are indicated in bold, * $p<0.05$, ** $p\leq0.001$, with direction of change indicated by arrow. som phs, somites post-heatshock.

Table S3. Templates for riboprobes

Probe name	Source of plasmid or template*
mespb	Sawada, A., Fritz, A., Jiang, Y.J., Yamamoto, A., Yamasu, K., Kuroiwa, A., Saga, Y., and Takeda, H. (2000). Development *127*, 1691-1702.
myoD	Weinberg, E.S., Allende, M.L., Kelly, C.S., Abdelhamid, A., Murakami, T., Andermann, P., Doerre, O.G., Grunwald, D.J., and Riggleman, B. (1996). Development *122*, 271-280.
her7	Oates, A.C., and Ho, R.K. (2002). Development *129*, 2929-2946.
her1	Muller, M., v Weizsacker, E., and Campos-Ortega, J.A. (1996). Development *122*, 2071-2078.
dlC	Oates, A.C., and Ho, R.K. (2002). Development *129*, 2929-2946.
spt/tbx16	Ruvinsky, I., Silver, L.M., and Ho, R.K. (1998). Dev. Genes Evol. *208*, 94-99.
msgn1	Nested primers: 1st PCR: Msgn-1F (GCCGCACCTGCACATTT) and Msgn1-4R (AACCTTCCTAACATAAAAAGCGAAC) 2nd PCR: Msgn1-2F (GCACCTGCACATTTCTCTAACC) and Msgn1-3RT7 (TAATACGACTCACTATAGGTCAGAGCATCTTTACAACTTGG)
fgfR1	Poss, K.D., Shen, J., Nechiporuk, A., McMahon, G., Thisse, B., Thisse, C., and Keating, M.T. (2000). Dev. Biol. *222*, 347-358.
fgf3	Furthauer, M., Reifers, F., Brand, M., Thisse, B., and Thisse, C. (2001). Development *128*, 2175-2186
fgf8	Furthauer, M., Thisse, C., and Thisse, B. (1997). Development *124*, 4253-4264.
pea3	Munchberg, S.R., Ober, E.A., and Steinbeisser, H. (1999). Mech. Dev. *88*, 233-236.
erm	As above
axin2	Weidinger, G., Thorpe, C.J., Wuennenberg-Stapleton, K., Ngai, J., and Moon, R.T. (2005). Curr. Biol. *15*, 489-500.
ntl	Schulte-Merker, S., van Eeden, F.J., Halpern, M.E., Kimmel, C.B., and Nusslein-Volhard, C. (1994). Development *120*, 1009-1015.

*All plasmids or templates available on request.